Accepted Manuscript

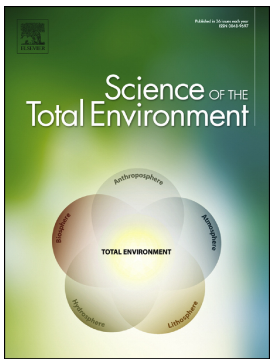

CFD modelling of air quality in Pamplona City (Spain): Assessment, stations spatial representativeness and health impacts valuation

Esther Rivas, Jose Luis Santiago, Yolanda Lechón, Fernando Martín, Arturo Ariño, Juan José Pons, Jesús Miguel Santamaría

PII: S0048-9697(18)33287-X
DOI: doi:10.1016/j.scitotenv.2018.08.315
Reference: STOTEN 28377

To appear in: *Science of the Total Environment*

Received date: 29 May 2018
Revised date: 20 August 2018
Accepted date: 23 August 2018

Please cite this article as: Esther Rivas, Jose Luis Santiago, Yolanda Lechón, Fernando Martín, Arturo Ariño, Juan José Pons, Jesús Miguel Santamaría , CFD modelling of air quality in Pamplona City (Spain): Assessment, stations spatial representativeness and health impacts valuation. Stoten (2018), doi:10.1016/j.scitotenv.2018.08.315

Title

CFD Modelling of Air Quality in Pamplona City (Spain): Assessment, Stations Spatial Representativeness and Health Impacts Valuation

Author names and affiliations

Esther Rivas[1], Jose Luis Santiago[1], Yolanda Lechón[2], Fernando Martín[1], Arturo Ariño[3], Juan José Pons[4], Jesús Miguel Santamaría[5]

[1]Atmospheric Pollution Division, Environmental Department, CIEMAT, Spain

[2]Energy System Analysis Unit, Energy Department, CIEMAT, Spain

[3]Environmental Biology Department, University of Navarra, Spain

[4]Department of History, History of Art and Geography, University of Navarra, Spain

[5]Chemistry Department, University of Navarra, Spain

Corresponding author

Esther Rivas

Atmospheric Pollution Division, Environmental Department,

CIEMAT, Av. Complutense 40, 28040 Madrid (Spain)

Phone: +34.653.77.21.83; E-mail: esther.rivas@externos.ciemat.es

Abstract

A methodology based on CFD-RANS simulations (WA CFD-RANS, Weighted Averaged Computational Fluid Dynamic-Reynolds–Averaged Navier–Stokes simulations) which includes appropriate modifications, has been applied to compute the annual, seasonal, and hourly average concentration of NO_2 and NO_X throughout the city of Pamplona (Spain) at pedestrian level during 2016. The results have been evaluated using measurements provided both by the city's network of air quality monitoring stations and by a network of mobile microsensors carried around by cyclists during their daily commutes, obtaining a maximum relative error lower than 30 % when computing NO_2 annual average concentrations.

The model has taken into account the actual city layout in three dimensions, as well as the traffic emissions. The resulting air pollution maps provided information critical for studying the traffic-related health effects of NO_2 and their associated external costs in the city of Pamplona and the spatial representativeness of the current network of air quality monitoring stations (it has not been carried out for an entire city to date). The developed methodology can be applied to similar cities, providing useful information for the decision-makers.

Keywords: CFD Model, City Scale, NO_2 Health Effects, Spatial Representativeness of Monitoring Stations, Urban Air Quality.

1. INTRODUCTION

The limit values for NO_2, NO_X and other air pollutants had already been established in 1999 by the European Directive 1999/30/EC (EC 1999) and, later, by a newer European Directive 2008/50/EC on ambient air quality and cleaner air for Europe (EC 2008). These air quality standards for NO_2 are currently being exceeded at many locations throughout Europe (EEA 2017a). There is thus substantial interest at the EU policy level in European studies about the health effects of current air pollution levels, including NO_2.

The impact of air pollution on human health is well documented through long- and short-term epidemiological cohort studies (Brunekreef & Holgate 2002; Brunekreef 2007). Air pollution from NO_2 in the cities has important effects on public health, summarized in two types of conditions. On the one hand, air pollution results in increased morbidity, especially by cardiovascular and respiratory diseases. McConnell et al. (2003) studied the long-term exposure to NO_2 and the appearance of bronchitis symptoms in asthmatic children, while Anderson et al. (2007) studied the associated short-term exposure to NO_2 and hospital admissions for respiratory diseases. On the other hand, exposure to NO_2 increases premature mortality, in terms of reduced life expectancy, as analysed by several studies (Samoli et al. 2006; Hoek et al. 2013).

However, despite the identified relationship between health effects and air pollution, recent epidemiological studies emphasized the difficulties in interpreting any health-related dataset when information on the intra-urban variability of pollution is not available (Beelen et al. 2008; Beelen et al. 2013; Jerrett et al. 2004). To consistently address health and regulatory issues related to urban air quality, both the spatial distribution and temporal variability of air pollution must be resolved at high resolution both in time (hours) and space (meters), and the contributions from different emission sectors must be assessed separately (Berchet et al. 2017).

One main source of air pollutants such as NO_X in cities is motor vehicles (Borge et al. 2014; Cyrys et al. 2012). These pollutants are emitted very close to the ground in the streets, being dispersed by the complex atmospheric circulation resulting from the perturbations that buildings induce on the general air flow. Therefore, the distribution of pollutants in cities gives rise to very complex patterns with high

concentration gradients. The European Air Quality Directive (EC 2008) specifies that "… a sampling point must be sited in such a way that the air sampled is representative of air quality for a street segment no less than 100 m in length at traffic-oriented sites…". Therefore, it is very important to verify the compatibility of the air quality stations measurements and the representativeness required by the Directive (Santiago et al. 2013; Martín et al. 2015; Santiago & Martín 2015).

Health-related effects of air pollutants exposure lead to direct economic costs, such as health expenses, but also to indirect or external costs in the form of welfare loss. These damages are generally not adequately reflected in the price of the activities generating them and this fact results in a non-optimal allocation of resources and the occurrence of welfare losses (Bickel & Friedrich 2005). These societal damages should be quantified when making decisions about policies to address air quality problems. Externalities from air pollution have been studied mainly in the framework of cost-benefit analysis of air quality policies (Holland 2014; EC 2013; U.S. EPA 2011; Larsen 2014) and such studies have become the bases of air quality policy design in Europe, the US and other countries. Usually these assessments conclude that benefits in terms of improved health outweigh the costs by a large margin.

Urban air quality can be simulated by means of mesoscale models, however their spatial resolution (around 1 km^2) makes not possible to resolve the high pollutant gradients observed in the streets. Therefore, microscale models are necessary. Parameterized microscale models such as OSPM (Berkowicz, 2000), SIRANE (Soulhac, 2011) or ADMS-URBAN (Di Sabatino et al., 2008) has been applied to simulate urban air quality. They are based on semi-empirical assumptions about the relation between the flow and dispersion of pollutants, within and out of the streets, and the urban morphology. Nevertheless, CFD models solve momentum and transport equations around complex geometries, as urban environments. The advantage of CFD models versus parameterized models is their capability to deal with complex shaped walls or boundaries using flexible fine-scale grids. Thus, wind flow and pollutant dispersion can be resolved around the buildings however, their computational cost is higher. This study is focused on the average pollutant concentrations over long time periods. The developed CFD methodology for this purpose makes possible to resolve hypothetical meteorological conditions using the existing CFD simulations, avoiding the handicap of the associated computational costs (as long as CFD simulations have been run and stored in a database previously).

In previous works, other authors have already used the CFD modelling to simulate NO_X and NO_2 concentrations in urban environments with high spatial resolution. For example, Santiago et al. (2017b) and Buccolieri et al. (2018), simulated NO_X concentrations in the streets of different cities under several meteorological scenarios and Borge et al. (2018) modelled NO_2 concentrations in a zone of Madrid (Spain) during a high pollution episode coupling mesoscale and CFD models but no considering a chemical scheme. Although the computational costs are higher, there are also some studies carried out CFD simulations of NO_2 concentrations in urban environments taking into account chemical reactions (Kwak et al., 2014; Sanchez et al., 2016; Santiago et al., 2017a). Those concluded that, during cold seasons, the obtained results agree with experimental measurements without considering the NO_X-O_3 chemistry. Other studies in which NO_X maps over long time of periods using similar methodologies are computed are: Parra et al. 2010; Santiago et al. 2011; Santiago et al. 2013; Santiago et al. 2017b; Sanchez et al. 2017. Between them, those of Parra et al. (2010) and Santiago et al. (2017b) are focused on a specific area of this city: the district of Plaza de la Cruz, but specific air quality studies throughout Pamplona was only carried out by Navarra Government by means of the measures of the network of air quality stations (GN, 2018). Concerning the use of CFD models to estimate the population exposure, few studies have been carried out yet. For example, Amorim et al. (2013) computed the individual exposure of students to the CO in an urban area with vegetation. In this study, the main objective was to evaluate the benefits by the trees over the mean exposure of students in their daily routes.

The objective of this work is to model the dispersion of pollutants in the streets, squares and parks of Pamplona (Spain), generating distribution maps of NO_X and NO_2 concentration at a high spatial resolution in the city. These maps would be useful to: 1) assess air quality in the whole city; 2) analyse the spatial representativeness of the network of air quality monitoring; and 3) compute the health impact of NO_2 concentrations. This objective is one of the main tasks framed within the LIFE + RESPIRA (LIFE13 ENV/ES/000417) European project.

For this purpose, representative concentration data spanning long time periods (e.g. annual and seasonal averages) were required. CFD modelling and a numerical methodology based on CFD-RANS simulations were applied to obtain the annual and seasonal average concentration maps of NO_2 and NO_X and the time-evolution of the annual and seasonal averaged days at pedestrian level during 2016. It is the first time that a methodology like this is applied to an entire city. It can be applied to similar cities, providing useful information for the decision-makers.

The numerical results were evaluated with experimental data from air quality monitoring stations and microsensors carried by cyclists traveling through Pamplona.

2. CASE STUDY AND EXPERIMENTAL DATA

2.1. Description of the area and the air quality/meteorology monitoring network.

Pamplona is the capital city of Navarra, a Spanish region located in the north of the Iberian Peninsula (Fig. 1 a). The metropolitan area had 195650 inhabitants in 2016 (representing 31 % of the region) (INE, 2017) and is a medium-sized city, similar to 80 % of cities in Europe. The city lies in the centre of a basin at 449 m above sea level, surrounded by mountains to the north and opening towards a valley to the south. This physical geography influences the city's meteorology, climate and air quality.

Pamplona has a network of air quality monitoring stations, which consist of two urban background monitoring stations, named Iturrama and Rotxapea, located to the south and north of the city respectively (neighbourhoods 3 and 10 respectively, Fig. 1 c), and one traffic monitoring station, named Plaza de la Cruz (PC), located in the city centre (neighbourhood 8, Fig. 1 c), which collect data of O_3, SO_2, NO, NO_2, CO, NO_X and PM_{10} with a ten-minute interval.

In addition, Pamplona has two automatic meteorological stations, named GN and UPNA, located in the centre and to the south of the city respectively (Fig. 1 c), which collect data every ten minutes of temperature, relative humidity, global irradiance, insolation, precipitation and wind speed and direction. Measurements corresponding to 2016 are discussed below to better understanding the time variability of pollutant concentration in Pamplona and to set up suitable boundary conditions for the CFD model.

Fig. 1

The levels of global irradiance and temperature strongly affect the atmospheric processes since they influence the height of the mixing layer and the photochemical activity. Furthermore, airflows are modified by urban morphology depending on several factors such as the city's layout, streets orientation, building geometry, and building surface fraction, which influence the dispersion of pollutants through the streets, avenues and squares.

The main wind directions in Pamplona are NW and SE (Fig. 2 a), coincident with the basin axis. During 2016, the maximum hourly average global irradiances registered in the city centre were 800 $W \cdot m^{-2}$ during

summer and 300 $W \cdot m^{-2}$ during winter, and the average minimum temperature was 15º C and the maximum was 27º C in summer, while they were 4º C and 9º C respectively during winter (Fig. 2 b).

Fig. 2

The urban configuration of Pamplona varies greatly depending on the neighbourhood (Table 1). Depending on the neighbourhood, the mean building height (z_H) ranges from 9 m to 22 m; the maximum building height (Z_{max}) ranges from 27 m to 60 m and the building surface fraction (λ_b) (Stewart & Oke 2012) ranges from 8 % to 45 %.

Table 1

In Pamplona, the 48 % of the commuting is done by car (Monzón et al., 2016). According to the road features and the observed traffic intensity, in Pamplona the roads are classified (Fig. 3) as:

a. Arterials, which include the radial approaches to Pamplona and its ring road and serve as direct access or fast connections between the different parts of the city. Vehicles circulate without stopping and traffic levels are high.

b. Distributors, which criss-cross Pamplona and distribute the urban and interurban traffic. Short trips are predominant and traffic levels are intermediate.

c. Locals, which group the rest of the roads in the neighbourhoods, facilitating access to buildings (e.g. houses, schools, shopping areas, workplaces), parks, etc. Short trips are predominant and traffic intensities are low.

In addition to urban micrometeorology, distribution of pollutants is related to emission sources. Most of the NO_X traffic emissions are in the form of NO, which is later oxidized to NO_2 by means of photochemical reactions (Leighton, 1961). The NO_2/NO_X concentration ratio in many cities across Europe has increased over the past decade because of changes in the composition of vehicle fleets (raise in the proportion of diesel-engine vehicles) and the introduction of new exhaust technologies. According to the national emission inventory in the centre of Pamplona, it is estimated that approximately 82 % of total NO_X emissions at Pamplona are due to the traffic (MAPAM, 2017).

Fig. 3

2.2. Analysis of measured pollutant concentrations at air quality monitoring stations.

In Fig. 4 the comparison between PC, Rotxapea and Iturrama monitoring stations of the average daily evolutions of NO_X, NO_2, NO and O_3 concentrations for 2016 are shown.

Fig. 4

Two peaks of primary pollutant concentration (NO_X, NO_2 and NO) were observed, one at early morning (7 AM - 8 AM local solar time) and another in the late afternoon (7 PM – 8 PM) (Fig. 4). As expected, higher concentrations were measured in the traffic station. These peaks were related to rush hour of traffic, photochemistry activity and planetary boundary layer (PBL) height. Unlike NO and NO_X, the late afternoon peak of NO_2 at the traffic station was higher than that recorded in the early morning, probably due to a greater O_3 availability to produce NO_2 by titration (Leighton 1961). After 8 AM, concentrations decreased until they reached their lower levels between 3 PM and 4 PM. As it is well known, O_3 concentrations are relatively low in the early morning, increase about midday and peak at around 3 PM, when the NO concentrations are low. The times for the maxima of nitrogen oxides were the result of the combination of high emissions from traffic during the rush hours with shallow mixing layers or low-height thermal inversion. Chemical reactions such as titration also play a significant role in increasing the NO_2 concentrations depending on the availability of O_3.

Differences could be found between the summer and winter averages of the daily cycles of nitrogen oxides (Fig. 4 b and 4 c). The peaks of nitrogen oxides were much lower in summer due to the mixing processes (higher PBL height). Ozone reached a higher maximum during summer, compared to winter, resulting from higher global irradiance and temperature (see Fig. 2 b). The maximum was observed between 2 PM and 3 PM during the summer and between 3 PM and 4 PM during the winter, related to maxima of global irradiance and temperature (see Fig. 2 b), and coincidental with minima of NO and NO_2 (therefore, also the NO_X). There was a small decrease in O_3 concentration in the early morning (from 4 AM to 7 AM, during summer and from 5 AM to 8 PM, during winter), when larger amounts of NO_X are produced from traffic emissions. Therefore, as expected, in summer, the impact of photochemistry is more important to determine NO and NO_2 concentrations than in winter.

Finally, the ratio of annual and seasonal NO_2/NO_X ratios was analysed at both PC and Rotxapea monitoring stations in order to study the impact of atmospheric chemistry (Fig. 5.).

Fig. 5

Overall, the annual NO_2/NO_X ratio during daylight hours (8 AM to 8 PM) was similar between background (Rotxapea) and traffic (PC) stations, with a 5 % yearly difference (Fig. 6 a) and -2 % in winter (Fig. 6 b). However, in summer the ratio at the background station was higher by 20 % (Fig. 6 c). These results confirmed that during the warm season the effects of atmospheric chemistry were more important than in the cold season, resulting in uneven NO_2/NO_X ratios across the city. NO_X can be simulated by the CFD model as a non-reactive pollutant (Sánchez et al. 2016), and the observed ratios were used to transform NO_X concentrations into NO_2 concentrations without a chemical scheme implemented in the CFD model, as will be explained in the next section (§ 3.2). For cold seasons, this approach seems to be appropriate. However, for warm seasons when atmospheric chemistry should be significant, the use of the CFD model without chemistry can produce a deviation of roughly 20 % in the concentration estimates.

3. MODELLING APPROACH

In this section we describe the modelling approach: CFD model description and simulation setup (numerical domain, mesh and physical models) (§ 3.1), and the numerical methodology used to obtain the average maps by combining the different simulated scenarios (CFD results) (§ 3.2).

3.1. CFD model description and simulation setup.

The numerical domain has about 42 km^2 (Fig. 1 c), about 7.7 km x 5.4 km, and covers in excess the whole city (approx. 25.3 km^2). A 3D full-scale geometrical model has been constructed, which considers the actual average height of each building separately.

The computational grid is a combination of polyhedral (between $z_H = [0, 1.5 \cdot Z_{max}]$, Fig. 6, right) and tetrahedral (between $z_H = [1.5 \cdot Z_{max}, 7 \cdot Z_{max}]$, Fig. 6, right) cells. The tetrahedral region is generated from the polyhedral core, as an extrusion in the direction z_H, using a hyperbolic stretching law to compute the cell distribution growth in the direction of the extrusion. (10 layers with a stretching factor 1.3). This type of combination allows to save computational costs and is a good compromise when it comes to solving the atmospheric flow in the highest part of the domain. Instead, the polyhedral region is divided in two control volumes, CV_1 (between $z_H = [0, 1.25 \cdot Z_{max}]$, Fig. 6, right) and CV_2 (between $z_H = [1.25 \cdot Z_{max}, 1.5 \cdot Z_{max}]$, Fig. 6, right), whose typical resolutions are 5 m (in built-up zones) and 10 m (far from

buildings) respectively, Fig 6, left. In CV_1, the mesh includes further refinements in the narrowest streets and a prismatic layer of 1 m around all urban surfaces (ground and buildings), to capture the influence of those obstacles. The transition between the prismatic layer and the core is carried out gradually, maintaining a growth factor of 1.3. The vertical and horizontal dimensions, Fig. 6, right, have been set following the recommendations given by Franke (2007) and Di Sabatino et al. (2011). The total number of cells is 44.6×10^6.

Fig. 6

Numerical simulations are based on a steady state RANS approach with the Realizable $k-\varepsilon$ Two Layer model. The commercial software STAR-CCM+9.04.011® has been used (Siemens 2018). To simulate the dispersion of primary pollutants inside the city, transport equations for passive scalars have been included, i.e., no chemical reactions of the primary pollutants are assumed. These equations consider both the advection and diffusion terms. And, the diffusivity is proportional to the turbulent viscosity (μ_t), computed by the Realizable $k-\varepsilon$ model, and inversely proportional to the turbulent Schmidt number (Sc_t). This approach combined with the turbulent model has been employed in other studies, such as Santiago et al. (2013), Santiago et al. (2017a, 2017b, 2017c).

Therefore, the pollutant is assumed to be a passive scalar emitted by the traffic close to the ground in roads of the streets and avenues. The pollutant source at each road has been assumed as a proportional value to its Annual Average Daily Traffic, AADT, (Fig. 7), and its length, and inversely proportional to the volume of the traffic emissions in such road. Then, CFD simulations do not provide the real concentrations but proportional values to real concentrations. In order to transform the computed values into real concentrations, a numerical methodology is applied.

Boundary conditions at buildings and ground surfaces are modelled considering the All Y+ wall hybrid treatment. Ground is considered a roughness wall with z_0= 0.05 m. 16 different wind directions are simulated. Inlet profiles for wind speed are logarithmic and for turbulent kinetic energy (k) and turbulence dissipation rate (ε) are computed by the following equations (Richards & Hoxey 1993):

$$u(z) = \frac{u_*}{\kappa} \cdot ln\left\{\frac{z+z_0}{z_0}\right\}, k = \frac{{u_*}^2}{\sqrt{C_\mu}}, \varepsilon = \frac{{u_*}^3}{\kappa \cdot (z+z_0)}$$

where u_* is the friction velocity, z_0 is the roughness length, C_μ is a model constant (= 0.09) and κ is von Karman's constant (κ= 0.4). For these simulations, u_*= 0.24 m·s^{-1} is used. This value indicates a velocity logarithmic profile at inlet with 3.2 m·s^{-1} at 10 m.

These neutral atmospheric conditions (isothermal conditions) are usually used in CFD simulations. In these conditions, simulated pollutant concentrations are inversely proportional to wind speed, however, u_* value has no influence in the final results because the WA CFD-RANS methodology (§ 3.2) transforms simulated pollutant concentrations taken from CFD model at this velocity to modelled pollutant concentrations considering the measured wind speed.

Fig. 7

Several CFD-RANS studies have analysed the dependence of the pollutant concentration levels with the turbulent Schmidt number used in the turbulent mass transport equation (Di Sabatino et al. 2007; Tominaga & Stathopoulos 2007; Gromke et al. 2008; Vranckx et al. 2015; Gromke & Blocken 2015). Typical values range from 0.7 to 0.9 (Delaunay 1996; Baik et al. 2003; Kim & Baik 2003; Santiago et al. 2007; Tominaga & Stathopoulos 2007; Dejoan et al. 2010), although Tominaga & Stathopoulos (2007) pointed out that the optimum values range from 0.2 to 1.3 depending on the geometry and flow properties. For the set of CODACS experiments, Vranckx et al. (2015) observed that the optimum Sc_t depended on the case and, in general, ranged from 0.3 to 1.0. Before this work, a sensitivity analysis about the turbulent Schmidt number has been carried out (not showed here). The optimal value for this case was 0.7, which agrees other works (Spalding 1971; Li & Stathopoulos 1997; Wang & McNamara 2006).

3.2. Numerical methodology.

As unsteady simulations over long time periods are computationally extremely intensive, a numerical methodology based on Weighted Averaged of Computational Fluid Dynamic-Reynolds–Averaged Navier–Stokes (WA CFD-RANS) simulations was used (Parra et al. 2010; Santiago et al. 2011; Santiago et al. 2013; Santiago et al. 2017b; Sanchez et al. 2017), which includes the appropriate modifications. It consisted of 16 meteorological scenarios corresponding to as many different wind directions (sectors N, NNE, NE, ENE, E, ESE, SE, SSE, S, SSW, SW, WSW, W, WNW, NW, and NNW) with the same inlet velocity using steady-state CFD-RANS simulations. The inlet wind direction varied from 0º to 360º with an increment of 22.5º, i.e. sector N = 0º, NNE = 22.5º and so on. This methodology had previously been

only applied to small sections of a city such as a single quarter, and we expand it here to model the entire city.

In this case, the final average concentration maps are computed as a weighted sum of the simulated scenarios considering the wind patterns within the analysed periods. So, pollutant concentrations are computed assuming: 1) non-reactive primary pollutants, 2) thermal effects negligible in comparison with dynamical effects, and 3) pollutant concentrations depending only on emission sources and wind speed. The meteorological data during the study period were obtained from the GN station.

The average NO_X concentration maps were thus computed as,

$$C_M(t) = \left[\sum_{i=1}^{16} f_i(t) \cdot C_{CFD,i} \cdot \frac{u_M}{u_{ref,i}(t)}\right] \cdot E(t)$$

where $C_M(t)$ is the modelled average concentration at time t (time resolution was 1 h), i indicates the wind direction sector at inlet in CFD simulations, $f_i(t)$ is the statistical frequency of wind direction sector i at time t during the modelled period, $C_{CFD,i}$ is the concentration computed by CFD for the wind direction sector i (i.e. results from the corresponding steady state CFD-RANS simulation), $u_{ref,i}(t)$ the average wind speed of wind direction sector i measured at the GN meteorological station at time t during the modelled period, u_M the simulated inlet velocity and $E\,(t)$ an emission factor at time t during the modelled period.

$E\,(t)$ is an unknown parameter in our simulations (data about emissions are not available); therefore, it is fitted assuming that:

$$\overline{C_O(\vec{r_0}, t)} = C_M(\vec{r_0}, t)$$

where $\overline{C_O(\vec{r_0}, t)}$ is the measured average concentration at time t at PC monitoring station and $C_M(\vec{r_0}, t)$ the modelled concentration at time t.

NO_2 is a reactive pollutant but this methodology can only be applied for non-reactive pollutants. In addition, considering atmospheric chemistry in the CFD model as in Sanchez et al. (2016) was unaffordable for such a large domain. To solve this handicap, the measured average ratios NO_2/NO_X at time t at PC monitoring station during each period were applied to transform NO_X concentration maps as:

$$\left(C_M(t)\right)_{NO_2} = \left(C_M(t)\right)_{NO_X} \cdot \frac{\left(\overline{C_O(\vec{r_0},t)}\right)_{NO_2}}{\left(\overline{C_O(\vec{r_0},t)}\right)_{NO_X}}$$

This assumption was suitable during winter since it has been shown that during this season the effects of atmospheric chemistry are usually negligible, averaging less than 10 % (Santiago et al. 2017).

In this case, taking into account the small relative differences in annual and winter NO_2/NO_X ratios between monitoring stations (see § 2.1) and the very large computational cost that the application of an atmospheric chemistry model would have required, the assumption above described could be considered as a good compromise.

However, as mentioned earlier (§ 2.1) this assumption did not hold for summer, and therefore it was expected that the errors at the background monitoring station during this period due to the atmospheric chemistry would be higher by roughly 20 %.

Finally, the corresponding annual and seasonal averaged maps were computed as,

$$(C_M)_{NO_X \text{ or } NO_2} = \frac{1}{24} \cdot \sum_{j=1}^{24} C_M(t_j)$$

where $C_M(t_j)$ is the modelled average concentration at time t, and j indicates the hour.

3.3. Methodology to estimate health effects and related externalities.

The estimation of the damage caused by air pollution required a complete methodological process known as the impact pathway developed in the framework of the ExternE project series (Bickel & Friedrich 2005). This methodology offers an analytical framework capable of transforming the information related to the emission of different pollutants into a common unit: monetary units. The process consists in following the pollutants throughout all the phases, from their emission until they reach the receptors, causing them damage. The following stages can be distinguished:

a) Emission of pollutants.

b) Atmospheric concentration: estimating the concentrations of pollutants in the area of study.

c) Exposure of the population to the concentrations of NO_2 produced. A requirement is knowing the spatial and age distribution of the city's population.

d) Environmental impact. The estimation is carried out through the application of exposure-response functions that allow determination of the increase in the health endpoints caused by an increase in the atmospheric concentration of the pollutant.

e) Damage caused, which consists in estimating the value that the population attributes to the impacts caused by pollution. This estimation allows determining the deterioration of the wellbeing of the population because of the variation in the atmospheric quality induced by the pollution emitted by road traffic in the urban environment.

We followed the above methodology using the NO_2 concentration maps obtained through our modelling; the data of the Municipal Census of Inhabitants as the age-specific distribution of the population of the city of Pamplona in a grid of 100 x 100 m cells; and information from the literature about the incidence of diseases related to exposure to NO_2.

The health impacts were quantified through the exposure-response functions proposed by the World Health Organization (WHO 2013b), by applying the following formula to each cell in the domain:

$$I = C \times P \times R \times CRF \times V$$

where

I: Impact expressed as number of additional cases

C: Concentration of the pollutant

P: Population at risk

R: Incidence ratio

CRF: Concentration Response function or change in incidence per unit of concentration

V: Monetary valuation of the impact on health

The exposure concentration response functions used were those proposed by the WHO in the HRAPIE project (WHO 2013b):

1) Effects of long-term exposure to NO_2 on mortality in the population over 30 years of age. The WHO experts recommend the application of a linear CRF function that corresponds to a relative risk (RR) of 1.055 (confidence interval 1.031-1.08) for every 10 $\mu g \cdot m^3$ of annual mean concentration of NO_2. This

RR value was obtained from a meta-analysis by Hoek et al. (2013) and considers a threshold concentration of 20 $\mu g \cdot m^3$. The mortality rate was obtained from the Statistical Institute of Navarra for the entire province of Navarra and was 0.89 % for the year 2015 (NA-STAT, 2018).

2) Effects of long-term exposure to NO_2 on the onset of bronchitis symptoms in asthmatic children between ages 5 and 14. The WHO recommends the use of the results of McConnell et al. (2003), which calculate a RR of 1.021 (confidence interval 0.99-1.06) for every 1 $\mu g \cdot m^3$ of NO_2. The percentage of asthmatic children in the city of Pamplona was obtained from the data of the Primary Care Service of the Navarra Health Service for each of health district of the city. The prevalence of bronchitis symptoms in asthmatic children was considered as the average of the values in Migliore et al. (2009) and McConnell et al. (2003), being 21.1 % and 38.7 % respectively.

3) Effects of short-term exposure to increased levels of NO_2 in mortality. WHO recommends using the results of the APHEA-2 project (Samoli et al. 2006) covering 30 European cities and obtaining an RR value of 1.0027 (confidence interval 1.0026-1.0038) for every 10 $\mu g \cdot m^3$ of daily maximum 1-hour mean maximum concentration of NO_2.

4) Effects of short-term exposure to increased concentrations of NO_2 in hospital admissions for respiratory diseases. The WHO recommends the use of RR values from the study by Anderson et al. (2007) of 1.018 (confidence interval 1.0115-1.0245) per 10 $\mu g \cdot m^3$ of average 24-hour mean daily maximum concentration. The base value for hospital admissions for respiratory diseases was obtained from the WHO European Hospital Morbidity Database (WHO 2013a) and is 1.26 % for Spain.

Experts in the HRAPIE project classified the recommended exposure-response functions (CRFs) in two categories:

• Group A: CRFs that allow a robust quantification of the effects. The last two functions are included in this category.

• Group B: CRFs for which there is more uncertainty about the accuracy of the data used to quantify the effects. The first two functions are included in this category.

In this evaluation both the functions of group A and those of group B were used, so that a limited set of impacts based on the sum of the functions of Group A* was calculated first and then an extended set of impacts based on the sum of the functions of Group A* and Group B*.

The monetary valuation of these impacts is done by multiplying the impacts in physical terms by the unitary monetary value of each condition to health. These unit values aim to capture the total economic impact of health impacts and include health costs, lost productivity and aversion to poor health or reduced life expectancy. The monetary values used in this study were those proposed by Holland in the cost benefit analysis of the Clean Air Package of the European Commission (Holland 2014) after converting them to 2015 Euros through the Consumer Price Index, CPI (Table 2).

Table 2

An analysis of the uncertainty of these calculations was made considering the 95 % confidence interval reported by the WHO for each of the RRs. However, other sources of uncertainty derived from the modelling of pollution distribution, population exposure, health data reference rates or monetary valuation were not included.

One limitation of this study was that it considers that exposure is correlated to outdoor air pollution in the area of residence for the population. However, exposure is dynamic and depends on individual behaviour and how long individuals stay at home, at work, or outdoors somewhere else throughout the city.

4. RESULTS

The annual and seasonal average NO_2 and NO_X concentration maps throughout the city of Pamplona at pedestrian level during 2016, as well as the corresponding hourly average maps (i.e. annual, winter, spring, summer and autumn) were computed as previously described (§ 3.2). As an example, the high-resolution average annual NO_X maps at three different hours are shown in Fig. 8.

Fig. 8

As shown in Fig. 4, the highest levels of NOx (>> 200 $\mu g \cdot m^3$) occurred during peak traffic hours: 8 AM and 8 PM. As expected, the modelled maps (Fig. 8) show the highest concentrations along interurban, arterial and distribution roads (commonly multi-lane roads) (Fig. 3), corresponding to the observed traffic levels (intermediate and high) and where vehicles circulate faster. Also, high NOx (> 200 $\mu g \cdot m^3$) levels are observed at crossroads and roundabouts and, on the contrary, significantly lower levels are observed inside parks and gardens (< 20 $\mu g \cdot m^3$). However, there were also high concentrations along local streets in neighbourhood 8 (Fig. 1c) where the observed traffic levels were lower. This neighbourhood is

characterized by relatively narrow streets configured as street-canyons and having reduced ventilation. In addition, streets and avenues with high traffic surround this central neighbourhood. Here, in the most polluted places, and particularly during peak hours, the limit values set by the European Directive could be exceeded.

Finally, another remarkable feature observed in the NOx maps are the strong spatial gradients observed between roads and sidewalks, even between both sidewalks of the same road.

4.1. Model evaluation against experimental data from air quality monitoring stations (point measurements).

We compared modelled hourly NO_2 and NO_X concentrations with measurements from the background monitoring stations for annual and seasonal average days (Fig. 9).

Fig. 9

The simulated annual average of the daily cycle of NO_X concentrations (Fig. 9 a and 9 b) and the seasonal averages (Fig. 9 c and 9 d) were a good fit over the observations from both stations, especially during daytime hours (from 8 AM to 8 PM, local solar time), although there was some underestimation at night (8 PM to 8 AM, local solar time). The daily concentration peaks at 8 AM and 8 PM (see Fig.4) were slightly underestimated at the Rotxapea station but fit very well the Iturrama station. It should be noted that the Rotxapea station is located in a neighbourhood highly influenced by the topography (it lies at a lower altitude near the river bank, while the other stations are higher up in the city's plateau), which was not considered in the model (see more details in the next section). The reduced predictive power during the night (coincidental with lower overall concentrations) suggested that neutral inlet profiles were not appropriate to simulate night-time hours when the vertical transport of pollutants is also reduced.

Chang & Hanna 2004 recommended the use of statistical parameters such as the correlation coefficient (R), the normalized mean square error (NMSE), the fractional bias (FB) and the fraction of prediction within a factor of two of observations (FAC2) to evaluate the performance of the model with the observations (see Appendix for definitions). A perfect model would have R, FAC2 = 1 and NMSE, FB = 0. Table 3 shows these statistical parameters for the NO_X. In general, there is a good agreement for all cases. The correlation coefficients (R) are high for all cases and, in general, the acceptance criteria for urban applications established as NMSE<~0.6, |FB|<~0.67, and FAC2>~0.3 by Hanna & Chang (2012)

can be verified. The maximum absolute and relative errors (not shown here) hardly ever occur during daytime hours, which is the time frame of special interest as it is the most associated to the population's outdoor exposure. Note that the positive FB values indicate a general model underestimation which in our case is clearly driven by the nocturnal results.

Table 3

Fig. 10

The annual and seasonal extremes (summer and winter) NO_2 concentrations for the Rotxapea station are shown in Fig. 10. In general, results were similar to those of NO_X. This was expected since the NO_2/NO_X ratios assumed in this model (corresponding to the PC station) for winter and for the full year were well suited to those observed at Rotxapea during daytime (Fig. 6 b and 6 a). All results verify the acceptance criteria established by Hanna & Chang (2012) although the worst correlation was obtained for summer (Table 4).

Table 4

Finally, modelled annual and seasonal average NO_2 and NO_X concentration maps were compared with measurements from the background monitoring station. The absolute and relative differences (see Appendix for definitions) are shown in Table 5. Modelled concentrations were slightly underestimated in all cases.

Table 5

While the results of the comparison are not perfect, they nonetheless indicate a good agreement that validates the methodology, given that a more accurate CFD simulation (i.e. including atmospheric chemistry) for such a large domain, long time and high resolution was unfeasible and that the legal error allowed for the measurements by the European Air Quality Directive (EC 2008) is approx. 20 % of relative error. We obtained a maximum relative error lower than 30 % when computing annual average concentrations, even though chemistry module is not included.

4.2. Model comparison against experimental data from cyclists with microsensors (distributed measurements).

During the LIFE+RESPIRA project, volunteer cyclists carrying microsensors recorded O_3, NO, NO_2, CO and PM (PM_{10}, $PM_{2.5}$ and PM_1) concentration data from about 13 million georeferenced data points (processing by suitable big data techniques), Fig. 1 b, over two years. Measuring low-level pollutants with mobile air quality sensors is challenging because at low gas concentrations, the applied technology and the sensors exhibit poor signal-to-noise ratio and high sensitivity to interference (Mijling et al., 2017). Furthermore, it was observed scant robustness and reproducibility despite using one the most reliable low-cost microsensors available on the market (Afshar-Mohajer et al., 2017). Besides, many of the detected errors proved impossible to correct, and such data was therefore conservatively marked as potentially invalid (5 million georeferenced data points were used in the analysis).

After very significant effort developing appropriate techniques, the researchers of LIFE+RESPIRA project were able to improve the signal quality and the intercalibration of sensors by approximately one order of magnitude (Santamaría et al., 2017). Finally, these experimental data were hourly segmented and spatially-averaged the pools in 50 × 50 m cells. This cell size is related with the sampling period (10 s) and the average speed of the cyclist, 5 $m \cdot s^{-1}$. We used these spatially-averaged hourly maps of annual NO_2 concentration at pedestrian respiration level during 2016 for the CFD model comparison.

Some limitations were associated to these experimental data, namely:

1) All these data points came from roads, streets, and other areas accessible to cyclists.
2) Measurements from cyclists unavoidably carried some spatial uncertainty as they moved, due both to the intrinsic accuracy of the GPS devices and the several meters that cyclist would move during the 10-second averaging period.
3) Finally, the amount of data points per cell and hour was rather uneven as the cyclists were actually collecting during their usual commutes, which were naturally patterned over space and time according to their needs. Therefore, some cells or times had few data points especially in the deep of the night.

To overcome these limitations during the comparison of the CFD model, we pooled and averaged the experimental data by hour and by neighbourhood and compared these averages with the corresponding hourly and neighbourhood averages obtained from the CFD model.

Neighbourhoods 5, 6, 7, 8, 10, 11, 12 and 13 (Fig. 1 c) were the most suitable for this comparison since they were the least affected by the topography, corresponding to the continuous central area which lies in

a plateau elevated over the surrounding peripheral quarters some 15-35 m lower and bounded by the three rivers that traverse the city (neighbourhoods 1, 2, 3, 4 and 9). Additionally, in neighbourhood 1 there is also one isolated hill. This topographic inhomogeneity can influence the atmospheric flows in different ways. For example, for the NW wind direction (which is quite frequent in Pamplona, see § 2), the central plateau and its glacis-type slopes can act as a barrier to the transport of atmospheric pollutants coming from the lower peripheral areas located windward.

As the simplified CFD model we used assumed a flat terrain, we expected that the comparison with experimental data would produce a better fit for the plateau neighbourhoods than for the surrounding, lower and topographically irregular neighbourhoods, for which the model could underestimate the experimental measurements according to the wind configuration. This was indeed confirmed for the windward neighbourhoods 1 and 4.

Neighbourhood 3 (Rotxapea) had been used for the model comparison despite belonging to the low, windward quarters because its air quality station is located in the centre of the neighbourhood surrounded of buildings and, thus, its measurements are not as influenced by the topography as measurements from cyclists, which are distributed throughout all neighbourhood. About neighbourhood 7 (corresponding to the historic centre of the city, with several streets closed to traffic), despite not being so influenced by the topography, has neither been considered in the experimental model comparison because no reliable AADT data was available.

Firstly, at each neighbourhood, modelled and observed annual average daily cycles of NO_2 concentration are compared.

Fig. 11

In Fig. 11, results at neighbourhoods 8 and 10 are shown as example. The simulated concentrations fit well the observations in both cases. The observed time evolutions are well captured by the model despite of some overestimations during day-time hours (from 8 AM up to 8 PM, local solar time). The first daily concentration peak (at 8 AM) is underestimated at neighbourhood 10 but fits very well at neighbourhood 8, and the second (at 8 AM), is in good agreement at both neighbourhoods.

To evaluate the temporal performance of the model with the observations, the statistical parameters described by Chang & Hanna 2004 are computed for each neighbourhood (see Table 6). As it can be

appreciated, there is a good agreement in all cases and the acceptance criteria of Hanna and Chang (2012) are fulfilled. Best results seem to be for neighbourhoods 8 and 13.

Table 6

Secondly, the modelled and observed NO_2 annual average-concentrations are compared at all considered neighbourhoods (5, 6, 8, 10, 11, 12 and 13, which represent the 53 % of total area of the city), Fig. 12.

Fig. 12

Results indicate that, in average, the observed concentrations are slightly overestimated by the model, according to the previous results. To evaluate the spatial performance of the model with the observations, statistical parameters are computed (Table 7) for the selected neighbourhoods considering all together.

Table 7

In this case there is also a reasonable agreement between real and modelled values and the acceptance criteria established by Hanna & Chang (2012) are also fulfilled. The absolute and relative differences at all neighbourhoods are shown in Table 8.

Table 8

Taking into account the errors of the microsensors (greater than 20 % of relative error) and that it is unaffordable to carry out a more accurately CFD simulation (i.e. including the topography) in such great domain and for such period of time, besides to already mentioned in the previous section (including atmosphere chemistry), it is confirmed that the resulted average maps are good enough to consider the CFD modelling with the applied methodology suitable for computing annual average concentrations where the relative errors are lower than 30 %.

Finally, by means of these results, it is possible to compare the annual average of the daily cycle of NO_2 concentrations breathed by cyclists who have gone through neighbourhoods 8 and 10 during 2016 with the annual average of the daily cycle of concentrations recorded by their corresponding air quality monitoring stations (PC and Iturrama respectively) (Fig. 11). In both cases, despite cyclists and stations record practically the same values out of the daily concentrations peaks (out of 8 AM and 8 PM), they can record until a 30 % more than the stations around these hours. Therefore, the real exposure of the cyclists

to traffic related pollutants at peak hours is not well represented by the air quality monitoring stations of Pamplona.

In summary, considering the positive results of the model evaluation and comparison both, with point (§ 4.1.) as distributed (§ 4.2.) measurements respectively, the obtained average maps are reliable enough to carry out studies in the city of Pamplona from them. Nevertheless, in some neighbourhoods of the city (belonging to the peripheral zone) the obtained average maps seem to show certain underestimation in the atmospheric pollutant concentrations. These results are applied to study the traffic related NO_2 health effects and their associated externalities (§ 6) and to analyse the spatial representativeness of the air quality monitoring stations in the city (§ 5).

5. HEALTH EFFECTS AND ASSOCIATED EXTERNALITIES IN THE CITY OF PAMPLONA

We found that, in 2016, around 7 % of the population of Pamplona had been exposed to nitrogen oxides levels above the maximum of 40 $\mu g \cdot m^3$ recommended both by the European Union and by the WHO. This was in line with the findings of EEA (EEA 2017b) regarding the exceedance of air quality limit values in urban areas that found that in 2015, 7-9 % of urban population in the EU-28 was exposed to levels above the limits.

This level of exposure has been associated to various health effects that have been quantified, for the conditions existing in 2016, to 16 years of life lost, 111 hospital admissions for respiratory diseases, 141 additional cases of bronchitis in asthmatic children and 50 years of life lost due to long-term exposure to these increased levels of contamination (Fig. 13). The results of the uncertainty analysis performed are shown in the graph as error bars.

Fig. 13

These effects translate into medical costs and loss of well-being that are called external costs or externalities. Our results (Fig. 14) indicate a total of M€1.37 (0.83-1.91) if we only take into account the effects considered as A* (green in the graphs), and a total of M€4.85 (2.78-6.99) if we consider all the effects. The most important external costs are due to the reduction in life expectancy followed by hospital admissions due to respiratory problems and cases of bronchitis in asthmatic children.

Fig. 14

External costs due to health effects are distributed spatially as shown in Fig. 15 and are higher in areas where there is a larger concentration of pollutants and where the population density is higher.

Fig. 15

6. REPRESENTATIVENESS OF URBAN MONITORING STATIONS

The distribution of atmospheric pollutants in Pamplona is very heterogeneous as can be appreciated in Fig 8. Large differences of concentration between streets located very close each other and even between zones of the same street or sidewalk are observed. Thus, it is very important that, the air quality monitoring stations of network of the city are adequately distributed; in such a way their measures represent as much as possible the breathed air quality by the citizens of Pamplona. Considering also the requirements of spatial representativeness of the European Air Quality Directive (EC 2008) ("…the air sampled is representative of air quality for a street segment no less than 100 m in length at traffic-oriented sites…"), an air quality network with many monitoring stations could be more easily able to suitably represent air quality in urban environments, but it can be very expensive.

One direct application of the obtained pollutant concentration maps of this work is to assess the spatial representativeness of the Pamplona's air quality monitoring stations network.

The methodology of using CFD techniques to obtain detailed pollutant concentration maps around air quality monitoring stations has been already used by other authors (Santiago et al. 2013; Martín et al. 2015, Santiago & Martín 2015) but, for single stations and domains of approximately 1 x 1 km^2. Up to date, this has not been carried out for an entire city. The main advantage of using this type of techniques is that they can provide reliable maps at air pollutant concentrations pedestrian respiration level with high spatial resolution (few meters), although their computational cost is typically high.

In this section, to illustrate the usefulness of these results, first, the spatial representativeness of each air quality monitoring station of the Pamplona's network respect to NO_2 is calculated and discussed. For this purpose, the average annual NO_2 concentration map at pedestrian level (3 m height) is used and the spatial representativeness is assumed to the area around each station whose concentration differs less than 20 % of the average annual value registered by the station. This criteria has been used also in others

works (Santiago et al., 2013) for urban stations and with some additional criteria (Martín et al., 2015) for rural background stations in Spain.

Fig. 16

The spatial representativeness areas of background monitoring stations (Rotxapea and Iturrama, Fig. 16 b, c) for NO_2 are 33.42 % and 30.97 % respectively of the total areas of the neighborhoods. On the other hand, the traffic monitoring station (PC, Fig. 16 a) is 17.65 % of the total area of the neighborhood, being much less representative than the others due to its location, close to traffic. In addition, this neighborhood has streets and avenues with high emission sources and several street canyons (low λ_b, Table 1). This fact produces strong concentration gradients in this neighborhood and thus, a lower spatial representativeness of its monitoring station, PC.

But in any case, as shown in Fig. 16, the inhabited areas, in general, are well represented (gray zones) by these stations, meanwhile, the streets and avenues with higher traffic levels and the least built-up zones not. These areas present the largest (red zones) and smallest (blue zones) concentration values of the neighborhoods respectively.

In urban environments it is expected the people's activities develop more frequently around the inhabited areas, therefore obtaining the maximum spatial representativeness of these areas should be the main objective when locating their air quality monitoring stations.

Finally, the spatial representativeness of the network for the entire city of Pamplona for NO_2 is calculated as the union of the representativeness area of the three monitoring stations. The obtained value is 18.40 % respect to the total area. As it is shown in Fig. 17, most of the residential areas of Pamplona (gray zones) are well represented, but some important avenues and streets with higher NO_2 concentrations are not represented by any air quality station.

Hence, we could conclude that the quality of the breathed air by most of the citizens of Pamplona is acceptably represented by the network of air quality monitoring stations, but some important avenues and streets with higher NO_2 concentrations are not represented by any air quality station.

Fig. 17

7. CONCLUSIONS

In this paper, a methodology (WA-CFD-RANS) based on CFD simulations is applied to an entire medium city to compute the annual and seasonal average concentration maps of NO_X, including the time-evolution of these average days. In addition, it is modified by using the hourly experimental values of the NO_2/NO_X ratios from an air quality monitoring station in order to compute NO_2 concentration maps without implementing a chemistry model. Up to now, this implementation is unaffordable in such large domain due to computational cost. Anyway, the developed approach can be used for calculating annual averages and cold season averages (but not warm season averages). This is the first time that this methodology is applied to compute pollutant concentrations along a complete city.

CFD simulations are more time-consuming in comparison with parameterized models, however the developed methodology in this work allows to obtain average concentrations maps during long time periods combining CFD simulations. Therefore, the average concentrations maps under other meteorological conditions can be computed modifying the combination of existing CFD simulations (turning the process into no so time-consuming). In other words, a set of pre-run CFD simulations can be used to keep the advantage of CFD models but preventing its handicap of high computational costs.

The numerical results have been evaluated with all available measurements. Firstly, air quality monitoring stations are used for this objective. Annual and seasonal averaged NO_X concentrations are well reproduced at both monitoring stations, with a slight underestimation in Rotxapea station. This is due to the fact that it is located in a neighbourhood clearly influenced by the topography, which is not considered in the model. Concerning NO_2 concentrations, the errors increase because of the lack of a chemistry model. However, by using the experimental ratio of NO_2/NO_X taken from the traffic station, the model results can be considered appropriate with a maximum relative error lower than 30 % in the annual average concentration. Although the relevance and accuracy of the data coming from monitoring stations is greater than that of microsensors carried by cyclist (since they are collected, transmitted and processed following standardized processes), a comparison with these measurements is performed in order to do a more extensive comparison. The combination of analytical refinements, calibration experiments, and the availability of a very large mass of data, has allowed to provide reliable microsensors information for the CFD maps comparison (Santamaría et al., 2017). NO_2 hourly annual average concentrations spatially averaged neighborhood-by-neighborhood is analyzed obtaining a good agreement with experimental data.

As for comparison with station data, the differences are lower than the 30 %. Therefore, this methodology is able to reproduce the annual average NO_2 map within an assumable error of 30 %. These results could be applied to different purposes. In this paper, the results have been applied to analyze the spatial representativeness of air quality monitoring network of the city for NO_2. This is the first time that the spatial representativeness of all air quality monitoring stations within a whole city is computed by using CFD modelling with high spatial resolution. The results indicate the air quality network of Pamplona represents quite well the air quality of the city, although some streets with higher NO_2 concentrations and other areas far from emissions with low concentration are not well represented by the stations. The concentration measured by background stations represents more than 30 % of the area of its neighborhoods while the representativeness of traffic station is, as expected, lower, close to 18 %.

The results obtained from the quantification of impacts of NO_2 emissions by road traffic carried out show that around 7 % of the citizens of Pamplona have been exposed in 2016 to levels of nitrogen oxides contamination above of the maximum levels of 40 $\mu g \cdot m^3$ recommended both by the European Union and by the WHO. This is in line with the findings of EEA (EEA 2017b). This caused important impacts on health, which in economic terms represent a loss of between M€ 1.37 and M€ 54.85. These results can be used to inform the air quality policy making process in the city of Pamplona. The results depend on the studied city (morphology, emissions. population distribution, etc.), however the developed methodology can be extrapolated to other similar cities.

These results about the health effects evaluation provides valuable information to policy-makers in order to estimate the impact of air pollution on health and the monetary valuation of these impacts. However, this analysis has some limitations. These results are related with the maximum exposure (only outdoor) since it has been considered that exposure is correlated to outdoor air pollution in the residence area of the population. Nowadays, there is no available information about the urban behaviors of population and how long individuals stay at home, at work, or outdoors somewhere else throughout the city. Therefore, this relevant handicap needs to be overcome in the next future with other studies/analysis or models, developing in parallel with this.

This study shows the importance to obtain high-resolution maps of NO_2 concentration for different applications such as the evaluation of the health impact effects of air quality or the analysis of air quality monitoring networks (i.e. it can be used to design the network of air quality monitoring station in order to

their measurements will be spatially representative). Additionally, the developed methodology can be applied to simulate different air pollution mitigation strategies providing information about the improvement of air quality, health impact and the corresponding saving costs (i.e. it can be used to evaluate different mitigation strategies). Then, policy-makers could obtain valuable information to decide the better strategy to implement in each city.

ACKNOWLEDGEMENTS

This study has been supported by the project LIFE+ RESPIRA (LIFE13 ENV/ES/000417) funded by EU. Authors thank Extremadura Research Centre for Advances Technologies (CETA-CIEMAT) by helping in using its computing facilities for simulations. CETA-CIEMAT belongs to CIEMAT and the Government of Spain and is funded by European Regional Development Fund (ERDF).

APPENDIX. STATISTICAL PARAMETERS USED

The absolute error (AE) and relative error (RE) are defined as:

$$AE = C_p - C_o;\ RE[\%] = \frac{|C_p - C_o|}{C_o}$$

The correlation coefficient (R), the normalized mean square error ($NMSE$), the fractional bias (FB) and the fraction of prediction within a factor of two of observations ($FAC2$), are given by:

$$FB = \frac{(\overline{C_o} - \overline{C_p})}{0.5(\overline{C_o} + \overline{C_p})};\ NMSE = \frac{\overline{(C_o - C_p)^2}}{\overline{C_0} \cdot \overline{C_p}};\ R = \frac{\overline{(C_o - \overline{C_o})(C_p - \overline{C_p})}}{\sigma_{C_p}\sigma_{C_o}};$$

$$FAC2 = fraction\ of\ data\ that\ satisfy\ 0.5 \leq \frac{C_p}{C_o} \leq 2.0$$

where:

C_p: model predictions;

C_o: observations;

$\bar{C}$: average over the dataset; and

σ_C: standard deviation over the dataset.

Note that since FB measures only the systematic bias of a model, it is possible for a model to have predictions completely out of phase of observations and still have $FB = 0.0$ because of cancelling errors.

REFERENCES

Afshar-Mohajer, N. et al., 2018. Evaluation of low-cost electro-chemical sensors for environmental monitoring of ozone, nitrogen dioxide, and carbon monoxide. Journal of Occupational and Environmental Hygiene, 15(2), pp.87–98.

Amorim, J.H. et al., 2013. Pedestrian exposure to air pollution in cities: Modeling the effect of roadside trees. Advances in Meteorology, 2013.

Anderson, H.R. et al., 2007. Quantitative systematic review of short term associations between ambient air pollution (particulate matter, ozone, nitrogen dioxide, sulphur dioxide and carbon monoxide), and mortality and morbidity. *Division of Community Health Sciences St George's - University of London*, 121 p.

Baik, J.-J., Kim, J.-J. & Fernando, H.J.S., 2003. A CFD model for simulating urban flow and dispersion. *Journal of Applied Meteorology*, 42(11), pp.1636-1648.

Beelen, R. et al., 2013. Development of NO_2 and NO_X land use regression models for estimating air pollution exposure in 36 study areas in Europe – The ESCAPE project. *Atmospheric Environment*, 72, pp.10-23.

Beelen, R. et al., 2008. Long-term effects of traffic-related air pollution on mortality in a Dutch cohort (NLCS-AIR Study). *Environmental Health Perspectives*, 116(2), pp.196-202.

Berchet, A. et al., 2017. A cost-effective method for simulating city-wide air flow and pollutant dispersion at building resolving scale. *Atmospheric Environment*, 158, pp.181-196.

Berkowicz, R., 2000. OSPM - a parameterised street pollution model. Environmental Monitoring and Assessment, 65, pp.323–331.

Bickel, P. & Friedrich, R., 2005. ExternE. Externalities of Energy. Methodology 2005 update. *Directorate-General for Research Sustainable Energy Systems - European Communities*, 287 p.

Borge, R. et al., 2018. Application of a short-term air quality action plan in Madrid (Spain) under a high-pollution episode - Part II: Assessment from multi-scale modelling. Science of the Total Environment, 635, pp.1574–1584.

Borge, R. et al., 2014. Emission inventories and modelling requirements for the development of air quality plans. Application to Madrid (Spain). *Science of The Total Environment*, 466-467, pp.809-819.

Brunekreef, B., 2007. Health effects of air pollution observed in cohort studies in Europe. *J Expo Sci Environ Epidemiol*, 17(2), pp. S61-5.

Brunekreef, B. & Holgate, S.T., 2002. Air pollution and health. *The Lancet*, 360(9341), pp.1233-1242.

Buccolieri, R. et al., 2018. The impact of trees on street ventilation, NOX and PM2.5 concentrations across heights in Marylebone Rd street canyon, central London. Sustainable Cities and Society, 41, pp.227–241.

Chang, J.C. & Hanna, S.R., 2004. Air quality model performance evaluation. *Meteorology and Atmospheric Physics*, 87(1-3), pp.167-196.

Cyrys, J. et al., 2012. Variation of NO_2 and NO_X concentrations between and within 36 European study areas: Results from the ESCAPE study. *Atmospheric Environment*, 62, pp.374-390.

Dejoan, A. et al., 2010. Comparison between large-eddy simulation and Reynolds-averaged Navier–Stokes computations for the MUST field experiment. Part II: effects of incident wind angle deviation on the mean flow and plume dispersion. *Boundary-layer meteorology*, 135(1), pp.133-150.

Delaunay, D., 1996. Numerical simulation of atmospheric dispersion in an urban site: Comparison with field data. *Journal of wind engineering and industrial aerodynamics*, 64(2-3), pp.221-231.

Di Sabatino, S. et al., 2011. COST 732 in practice: the MUST model evaluation exercise. International Journal of Environment and Pollution, 44(1/2/3/4), p.403.

Di Sabatino, S. et al., 2008. Flow and pollutant dispersion in street canyons using FLUENT and ADMS-Urban. Environmental Modeling and Assessment, 13(3), pp.369–381.

EC, 2013. Commission staff working document. Impact assessment. SWD (2013) 531 final. *European Commission*, 253 p.

EC, 1999. Council Directive 1999/30/EC of 22 April 1999 relating to limit values for sulphur dioxide, nitrogen dioxide and oxides of nitrogen, particulate matter and lead in ambient air. *Official Journal of the European Communities*, L 163(29/06/1999), pp.0041-0060.

EC, 2008. Directive 2008/50/EC of the European Parliament and of the Council of 21 May 2008 on ambient air quality and cleaner air for Europe. *Official Journal of the European Communities*, L152(11/06/2008), pp.0001-0044.

EEA, 2017a. Air quality in Europe — 2017 report. *European Environment Agency*, 80 p.

EEA, 2017b. Exceedance of air quality limit values in urban areas. *European Environment Agency*. Available at: https://www.eea.europa.eu/data-and-maps/indicators/exceedance-of-air-quality-limit-3/assessment-3.

Franke, J. et al., 2007. Best practice guideline for the CFD simulation of flows in the urban environment. *COST action*, 44, pp.1-52.

GN, 2018. INFORME ANUAL RED VIGILANCIA DE LA CALIDAD DEL AIRE DE NAVARRA 2017. On line at: http://www.navarra.es/NR/rdonlyres/E1A32A52-4889-4B4F-8FC5-7216A6DC604F/419485/Informeanual2017.pdf.

GN, 2016. Cartografía del Gobierno de Navarra. *Gobierno de Navarra - Nafarroako Gobernua*. Available at: ftp://ftp.cartografia.navarra.es/.

GN, 2008. Plan de movilidad urbana sostenible de la Comarca de Pamplona. *Gobierno de Navarra - Nafarroako Gobernua*, 90 p.

Gromke, C. et al., 2008. Dispersion study in a street canyon with tree planting by means of wind tunnel and numerical investigations–evaluation of CFD data with experimental data. *Atmospheric Environment*, 42(37), pp.8640-8650.

Gromke, C. & Blocken, B., 2015. Influence of avenue-trees on air quality at the urban neighborhood scale. Part I: Quality assurance studies and turbulent Schmidt number analysis for RANS CFD simulations. *Environmental Pollution*, 196, pp.214-223.

Hanna, S. & Chang, J., 2012. Acceptance criteria for urban dispersion model evaluation. *Meteorology and Atmospheric Physics*, 116(3-4), pp.133-146.

Hoek, G. et al., 2013. Long-term air pollution exposure and cardio-respiratory mortality: a review. *Environmental Health*, 12(1), pp.43-57.

Holland, M., 2014. Cost–benefit analysis of final policy scenarios for the EU clean air package - Version 2. *Environmental Measurement Research Corporation*, 68 p.

INE, 2017. Cifras oficiales de población de los municipios españoles: Revisión del Padrón Municipal. *Instituto Nacional de Estadística - Gobierno de España*. Available at: http://www.ine.es/dynt3/inebase/index.htm?padre=525.

Jerrett, M. et al., 2004. A review and evaluation of intraurban air pollution exposure models. *J Expo Anal Environ Epidemiol*, 15(2), pp.185-204.

Kim, J.-J. & Baik, J.-J., 2003. Effects of inflow turbulence intensity on flow and pollutant dispersion in an urban street canyon. *Journal of Wind Engineering and Industrial Aerodynamics*, 91(3), pp.309-329.

Kwak, K.H. & Baik, J.J., 2014. Diurnal variation of NO_X and ozone exchange between a street canyon and the overlying air. Atmospheric Environment, 86, pp.120–128.

Larsen, B., 2014. Air pollution assessment paper. *Copenhagen Consensus Center*, 64 p.

Leighton, P.A., 1961. *Photochemistry of air pollution*, Academic Press.

Li, Y. & Stathopoulos, T., 1997. Numerical evaluation of wind-induced dispersion of pollutants around a building. *Journal of Wind Engineering and Industrial Aerodynamics*, 67-68, pp.757-766.

MAPAM, 2017. Datos adicionales de emisiones. *Ministerio de Agricultura, Pesca, Alimentación y Medioambiente - Gobierno de España*. Available at: http://www.mapama.gob.es/es/calidad-y-evaluacion-ambiental/temas/sistema-espanol-de-inventario-sei-/datos-adicionales.aspx.

Martín, F. et al., 2015. FAIRMODE Spatial representativeness feasibility study - JRC Technical Report EUR 27385 EN. *Joint Research Centre - European Commission*, 82 p.

McConnell, R. et al., 2003. Prospective study of air pollution and bronchitis symptoms in children with asthma. *American journal of respiratory and critical care medicine*, 168(7), pp.790-797.

Migliore, E. et al., 2009. Respiratory symptoms in children living near busy roads and their relationship to vehicular traffic: results of an Italian multicenter study (SIDRIA 2). *Environmental Health*, 8(1), p.27.

Mijling, B. et al., 2018. Field calibration of electrochemical NO2 sensors in a citizen science context. Atmospheric Measurement Techniques, 11(3), pp.1297–1312.

Monzón, A. et al., 2016. Observatorio de la Movilidad Metropolitana - Informe OMM 2014. *Ministerio de Agricultura, Alimentación y Medioambiente - Gobierno de España*, 98 p.

NA-STAT, 2018. Información estadística. Población y demografía. *Instituto de estadística de Navarra - Gobierno de Navarra*. Available at: https://administracionelectronica.navarra.es/GN.InstitutoEstadistica.Web/informacionestadistica.aspx?R=1&E=1.

Parra, M.A. et al., 2010. A methodology to urban air quality assessment during large time periods of winter using computational fluid dynamic models. *Atmospheric Environment*, 44(17), pp.2089-2097.

Richards, P.J. & Hoxey, R.P., 1993. Appropriate boundary conditions for computational wind engineering models using the k-ϵ turbulence model. *Journal of Wind Engineering and Industrial Aerodynamics*, 46-47, pp.145-153.

Di Sabatino, S. et al., 2007. Simulations of pollutant dispersion within idealised urban-type geometries with CFD and integral models. *Atmospheric Environment*, 41(37), pp.8316-8329.

Samoli, E. et al., 2006. Short-term effects of nitrogen dioxide on mortality: an analysis within the APHEA project. *European Respiratory Journal*, 27(6), pp.1129-1138.

Sanchez, B. et al., 2016. CFD modelling of reactive pollutant dispersion in simplified urban configurations with different chemical mechanisms. *Atmospheric Chemistry and Physics*, 16(18), pp.12143-12157.

Sanchez, B. et al., 2017. Modelling NOx concentrations through CFD-RANS in an urban hot-spot using high resolution traffic emissions and meteorology from a mesoscale model. *Atmospheric Environment*, 163, pp.155-165.

Santamaría, J.M. et al., 2017. Book guide: REDUCTION OF EXPOSURE OF CICLYSTS TO URBAN AIR POLLUTION.

Santiago, J.L. et al., 2017a. Evaluation of a CFD-based approach to estimate pollutant distribution within a real urban canopy by means of passive samplers. *Science of The Total Environment*, 576, pp.46-58.

Santiago, J.L. et al., 2017b. The Impact of Planting Trees on NOx Concentrations: The Case of the Plaza de la Cruz Neighborhood in Pamplona (Spain). Atmosphere, 8(7).

Santiago, J.L., Martilli, A. & Martin, F., 2017c. On Dry Deposition Modelling of Atmospheric Pollutants on Vegetation at the Microscale: Application to the Impact of Street Vegetation on Air Quality. Boundary-Layer Meteorology, 162(3), pp.451–474.

Santiago, J.L., Martilli, A. & Martín, F., 2007. CFD simulation of airflow over a regular array of cubes. Part I: Three-dimensional simulation of the flow and validation with wind-tunnel measurements. *Boundary-layer meteorology*, 122(3), pp.609-634.

Santiago, J.L. & Martín, F., 2015. Use of CFD modelling for estimating spatial representativeness of urban air pollution monitoring sites and suitability of their locations. *Física de la Tierra*, 27, p.191.

Santiago, J.L., Martín, F. & Martilli, A., 2013. A computational fluid dynamic modelling approach to assess the representativeness of urban monitoring stations. *Science of The Total Environment*, 454-455, pp.61-72.

Santiago, J.L., Martín, F. & Matilli, A., 2011. Representativeness of urban monitoring stations. *In: 14th International Conference on Harmonisation Within Atmospheric Dispersion Modelling for Regulatory Purposes*, 19 p.

Siemens, 2018. CD Adapco - Star CCM+ User Guide (Only accessible by registry). *Siemens PLM Software Inc.* Available at: https://salesforce.industrysoftware.automation.siemens.com/WebkeyLogin/Authenticate3?url=https://salesforce.industrysoftware.automation.siemens.com:443/WebkeyLogin/SAMLAuth/alias/steveportal?token=fgLpi5Cu&id=GTV7h9O7.

Soulhac, L. et al., 2011. The model SIRANE for atmospheric urban pollutant dispersion; part I, presentation of the model. Atmospheric Environment, 45(39), pp.7379–7395.

Spalding, D.B., 1971. Concentration fluctuations in a round turbulent free jet. *Chemical Engineering Science*, 26(1), pp.95-107.

Stewart, I.D. & Oke, T.R., 2012. Local Climate Zones for Urban Temperature Studies. *Bulletin of the American Meteorological Society*, 93(12), pp.1879-1900.

Tominaga, Y. & Stathopoulos, T., 2007. Turbulent Schmidt numbers for CFD analysis with various types of flow field. *Atmospheric Environment*, 41(37), pp.8091-8099.

U.S. EPA, 2011. The benefits and costs of the clean air act from 1990 to 2020: Final report, Rev. A. *U.S. Environmental Protection Agency - Office of Air and Radiation*, 238 p.

Vranckx, S. et al., 2015. Impact of trees on pollutant dispersion in street canyons: A numerical study of the annual average effects in Antwerp, Belgium. *Science of the Total Environment*, 532, pp.474-483.

Wang, X. & McNamara, K.F., 2006. Evaluation of CFD Simulation using RANS Turbulence Models for Building Effects on Pollutant Dispersion. *Environmental Fluid Mechanics*, 6(2), pp.181-202.

WHO, 2013a. European hospital morbidity database. *Copenhagen, WHO Regional Office for Europe*. Available at: http://data.euro.who.int/hmdb/.

WHO, 2013b. Health risks of air pollution in Europe–HRAPIE project: Recommendations for concentration-response functions for cost-benefit analysis of particulate matter, ozone and nitrogen dioxide. *Copenhagen, WHO Regional Office for Europe*, 60 p.

Table 1

Number of Neighbourhood	*Area (km^2)*	*z_H (m)*	*Z_{max} (m)*	*λ_b (Adim.)*
1	3.7	11	27	12
2	1.5	11	39	30
3	1.3	15	30	29
4	3.8	9	33	11
5	2.2	19	57	17
6	1.4	21	57	17
7	0.6	17	36	45
8	2.7	16	51	20
9	1.1	13	27	8
10	2.4	22	60	12
11	0.7	22	51	13
12	2.5	17	45	13
13	1.4	11	33	12

Table 2

Impact	Unit cost	Unit
Mortality	68143.70	$Euros_{2015}$/year of life lost
Bronchitis	694.43	$Euros_{2015}$/case
Hospital admissions	2621.82	$Euros_{2015}$/case

Table 3

NO_X	Rotxapea				Iturrama			
	R	*NMSE*	*FB*	*FAC2*	*R*	*NMSE*	*FB*	*FAC2*
2016-average annual day	0.843	0.087	0.211	0.833	0.890	0.035	0.050	1
2016-average spring day	0.807	0.125	0.213	0.708	0.895	0.059	0.118	1
2016-average summer day	0.666	0.121	0.084	1	0.811	0.124	0.197	1
2016-average autumn day	0.826	0.110	0.250	0.833	0.860	0.047	0.048	1
2016-average winter day	0.814	0.180	0.348	0.708	0.817	0.079	0.116	0.875

Table 4

NO_2	Rotxapea			
	R	*NMSE*	*FB*	*FAC2*
2016-average annual day	0.683	0.118	0.254	0.792
2016-average spring day	0.699	0.146	0.261	0.708
2016-average summer day	0.492	0.221	0.291	0.708
2016-average autumn day	0.893	0.138	0.334	0.750

2016-average winter day	0.780	0.138	0.300	0.750

Table 5

AE[$\mu g \cdot m^{-3}$] / RE [%]	Rotxapea		Iturrama
	NO_X	NO_2	NO_X
2016-average annual map	-6.6 / 19.1	-4.4 / 22.5	-1.5 / 4.9
2016-average spring map	-4.4 / 19.3	-3.7 / 23.1	-2.4 / 11.1
2016-average summer map	-1.1 / 8.1	-2.7 / 25.4	-3.0 / 17.9
2016-average autumn map	-11.4 / 22.2	-7.7 / 28.6	-2.0 / 4.7
2016-average winter map	-14.9 / 29.7	-6.6 / 26.1	-4.8 / 11.0

Table 6

NO_2 Number of Neighbourhood	*R*	*NMSE*	*FB*	*FAC2*
5	0.675	0.124	-0.128	0.958
6	0.673	0.133	0.121	0.958
8	0.865	0.041	-0.095	1
10	0.639	0.107	-0.124	0.958
11	0.654	0.129	-0.197	0.917
12	0.715	0.111	-0.144	0.917
13	0.831	0.078	0.066	1

Table 7

NO_2	*R*	*NMSE*	*FB*	*FAC2*
2016-average annual map	0.565	0.040	-0.136	1

Table 8

AE[µg·m-3] / RE [%]	Number of Neighbourhood						
	5	*6*	*8*	*10*	*11*	*12*	*13*
2016-average annual map	7.6 / 29.0	0.3 / 1.0	4.2 / 15.0	5.6 / 21.3	6.8 / 25.6	6.2 / 28.7	-4.4 / 18.8

Table captions

Table 9: Neighbourhoods characteristics of Pamplona.

Table 10: **Monetary values of health conditions used in this study.**

Table 11: Statistical parameters comparing NO_X model results with measured data recorded at air quality monitoring stations (2016 annual and seasonal average days). All of them are dimensionless.

Table 12: Statistical parameters comparing NO_2 model results with measured data recorded at air quality monitoring stations (2016 annual and seasonal average days). All of them are dimensionless.

Table 13: Absolute and relative differences between NO_2 and NO_X model results and measured data recorded at air quality monitoring stations (2016 annual and seasonal average).

Table 14: Statistical parameters comparing modelled hourly NO_2 average-concentrations with experimental data from cyclists (2016 annual average day). All of them are dimensionless.

Table 15: Statistical parameters comparing modelled NO_2 average-concentrations with experimental data from cyclists (2016 annual average day). All of them are dimensionless.

Table 16: Statistical parameters comparing NO_2 model results with experimental data from cyclists (2016 annual average day).

Figure captions

Fig. 1: a) Pamplona's geographic situation (Source: Google Earth); b) cyclist tracks during 2016 (provided by University of Navarra); c) topographic map of Pamplona's City and the 13 main neighbourhoods (limited by means of continuous red lines), GN 2016, meteorological stations (green points), air quality monitoring stations (blue and yellow points, traffic and background stations respectively).

Fig. 2: a) Annual wind rose in UPNA station (Fig. 1) during 2016. b) Seasonal average of daily evolution of global irradiances and temperatures at GN station (the most central meteorological station of the city (Fig. 1) during 2016.

Fig. 3: Road network of Pamplona (GN, 2008).

Fig. 4: Average daily evolution of NO_X, NO, NO_2 and O_3 concentrations at monitoring stations for 2016: a) annual, b) winter and c) summer. Note that data of NO_2 and NO concentrations at Iturrama station were not available during 2016.

Fig. 5: Comparison between 2016 average daily evolutions of NO_2/NO_X at monitoring stations during: a) annual, b) winter, c) summer.

Fig. 6: Details of: left, CFD mesh model (buildings shaded in pink) and right, longitudinal plane section zoom and typical dimensions as function of the Z_{max}.

Fig. 7: Daily Average Traffic Intensity map in the city of Pamplona.

Fig. 8: High-resolution 2016 annual hourly average maps of NO_X concentration at: a) 8 AM, b) 2 PM, c) 8 PM, all of them local solar time. Red areas indicate NO_X concentrations greater than 200 $\mu g \cdot m^{-3}$.

Fig. 9: Comparison between modelled and observed hourly NO_X concentrations. Average annual day at station: a) Rotxapea, b) Iturrama. Seasonal average day at station: c) Rotxapea, d) Iturrama. Sp: spring; S: summer; A: autumn; W: winter.

Fig. 10: Comparison between modelled and observed hourly NO_2 concentrations at Rotxapea station: a) average annual day and b) average winter and summer day.

Fig. 11: Comparison between modelled and observed annual average daily cycles of NO_2 concentration at neighbourhood: 8 (left), 10 (right). In red, measurements from their corresponding air quality monitoring stations (PC and Iturrama respectively).

Fig. 12: Comparison between modelled and observed NO_2 average-concentrations. Average annual day at neighbourhoods 5, 6, 8, 10, 11, 12, and 13.

Fig. 13: Effects on health due to exposure to NO_2.

Fig. 14: External costs due to the health effects of NO_2.

Fig. 15: Distribution of calculated external costs.

Fig. 16: High resolution maps of NO_2 annual averaged concentration during 2016 at neighbourhoods: a) PC, b) Rotxapea y c) Iturrama. Grey zones show the areas with concentrations into +/- 20 % around the stations concentrations (stations represented by black points).

Fig. 17: High resolution map of NO_2 annual averaged concentration during 2016. Grey zones represent the spatial representativeness of the network (represented by black points) for all Pamplona's city.

Highlights

- CFD modelling of annual average NO_2 and NO_X maps throughout an entire city.
- Evaluation of modelled annual average concentrations with network station data.
- Comparison against average data recorded by mobile microsensors.
- Computation of spatial representativeness of monitoring stations of the city network.
- Assessment of health externalities arising from NO_2 in the whole city.

a)


PAMPLONA

b)

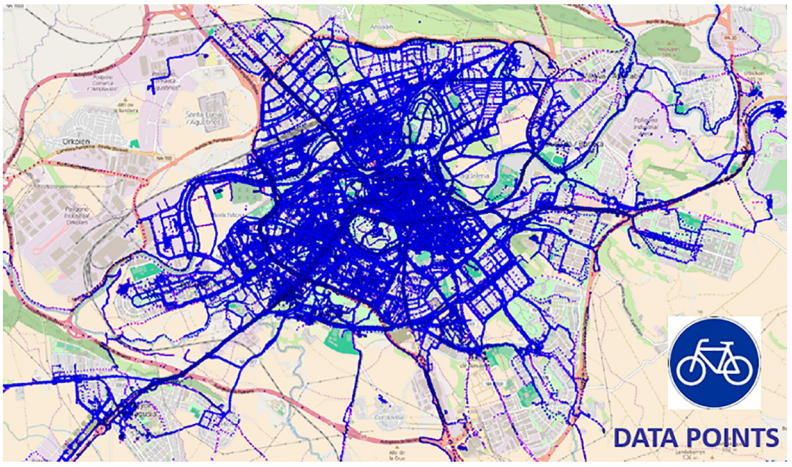
DATA POINTS

c)

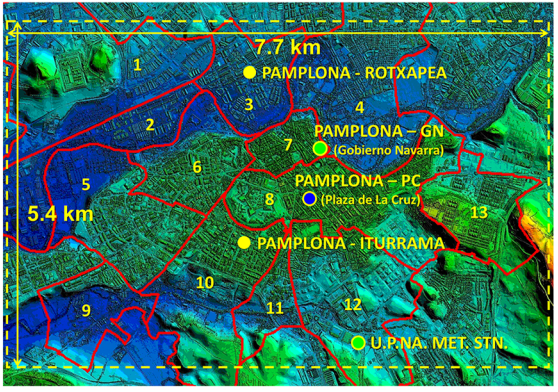
7.7 km
PAMPLONA - ROTXAPEA
PAMPLONA – GN
(Gobierno Navarra)
PAMPLONA – PC
(Plaza de La Cruz)
5.4 km
PAMPLONA - ITURRAMA
U.P.NA. MET. STN.
1
2
3
4
5
6
7
8
9
10
11
12
13

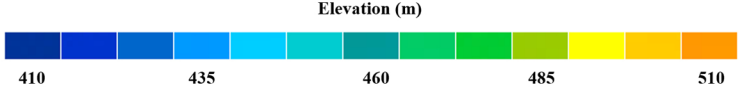
Elevation (m)
410
435
460
485
510

Figure 1

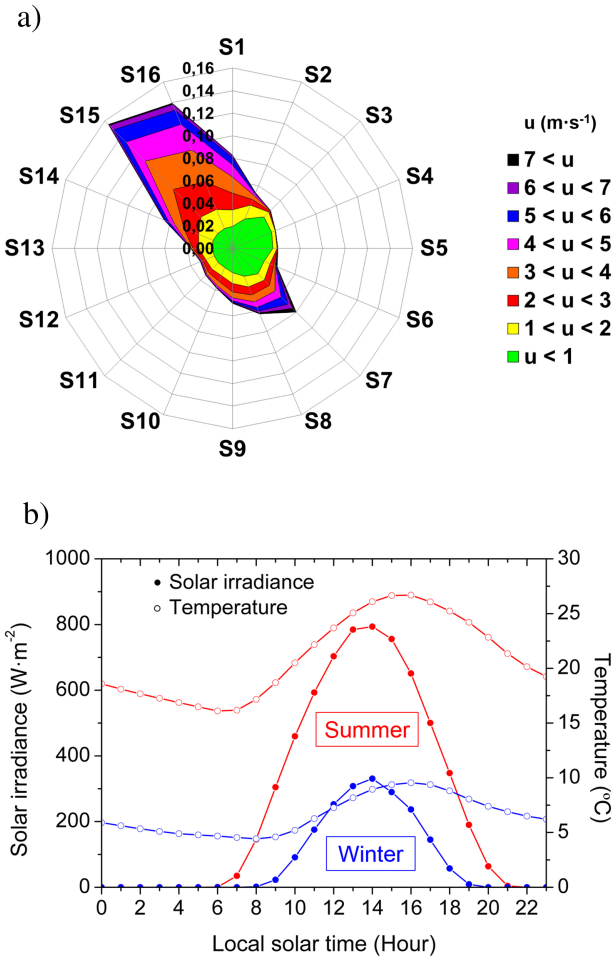
a)
S1
S2
S3
S4
S5
S6
S7
S8
S9
S10
S11
S12
S13
S14
S15
S16
0,16
0,14
0,12
0,10
0,08
0,06
0,04
0,02
0,00
u (m·s-1)
7 < u
6 < u < 7
5 < u < 6
4 < u < 5
3 < u < 4
2 < u < 3
1 < u < 2
u < 1
b)
Solar irradiance
Temperature
Summer
Winter
Solar irradiance (W·m-2)
Temperature (°C)
Local solar time (Hour)
0
200
400
600
800
1000
0
5
10
15
20
25
30
0
2
4
6
8
10
12
14
16
18
20
22

Figure 2

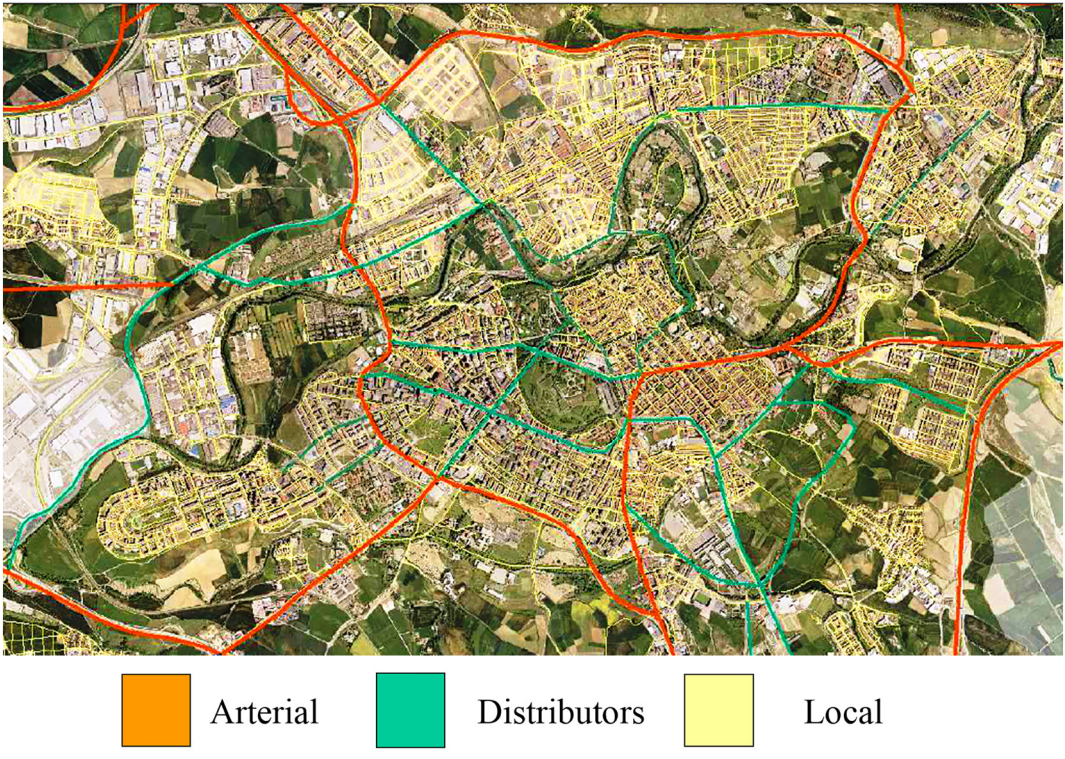

Figure 3

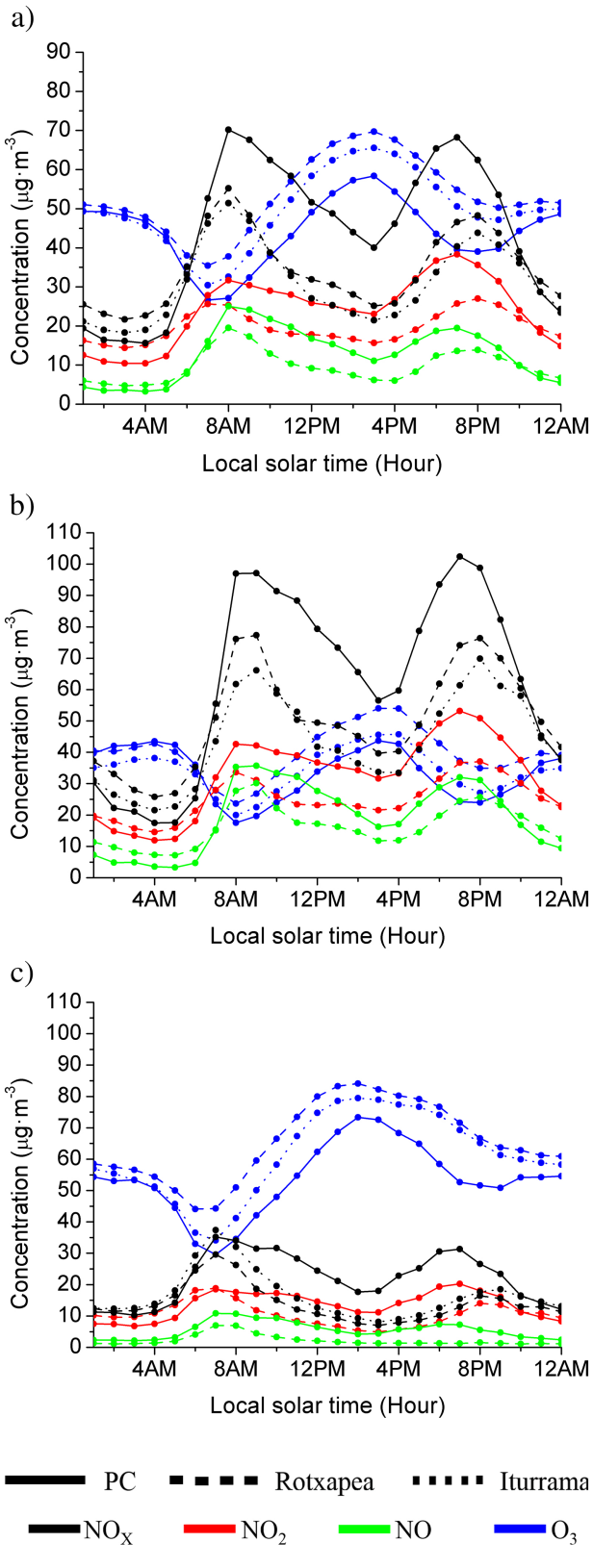
a)
Concentration (μg·m-3)
Local solar time (Hour)
4AM
8AM
12PM
4PM
8PM
12AM
b)
Concentration (μg·m-3)
Local solar time (Hour)
c)
Concentration (μg·m-3)
Local solar time (Hour)
PC
Rotxapea
Iturrama
NOX
NO2
NO
O3

Figure 4

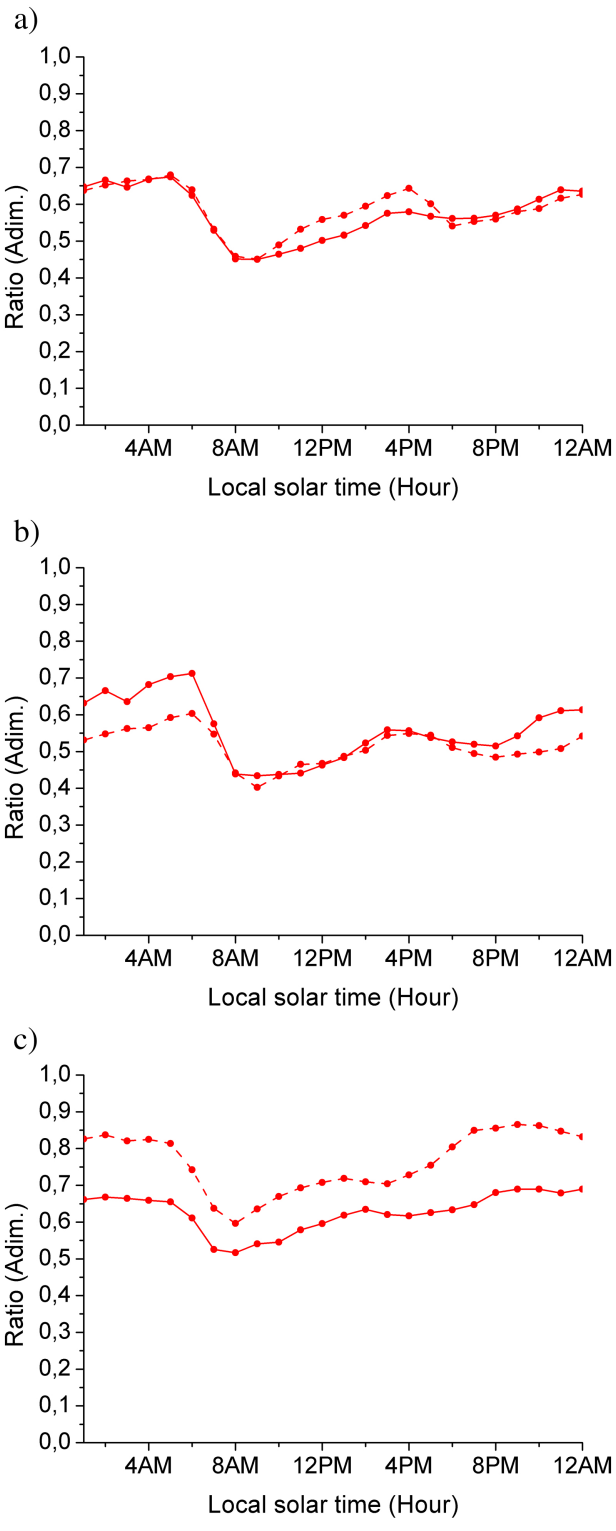
a)
Ratio (Adim.)
1,0
0,9
0,8
0,7
0,6
0,5
0,4
0,3
0,2
0,1
0,0
4AM
8AM
12PM
4PM
8PM
12AM
Local solar time (Hour)
b)
Ratio (Adim.)
Local solar time (Hour)
c)
Ratio (Adim.)
Local solar time (Hour)
PC_2016
Rotxapea_2016

Figure 5

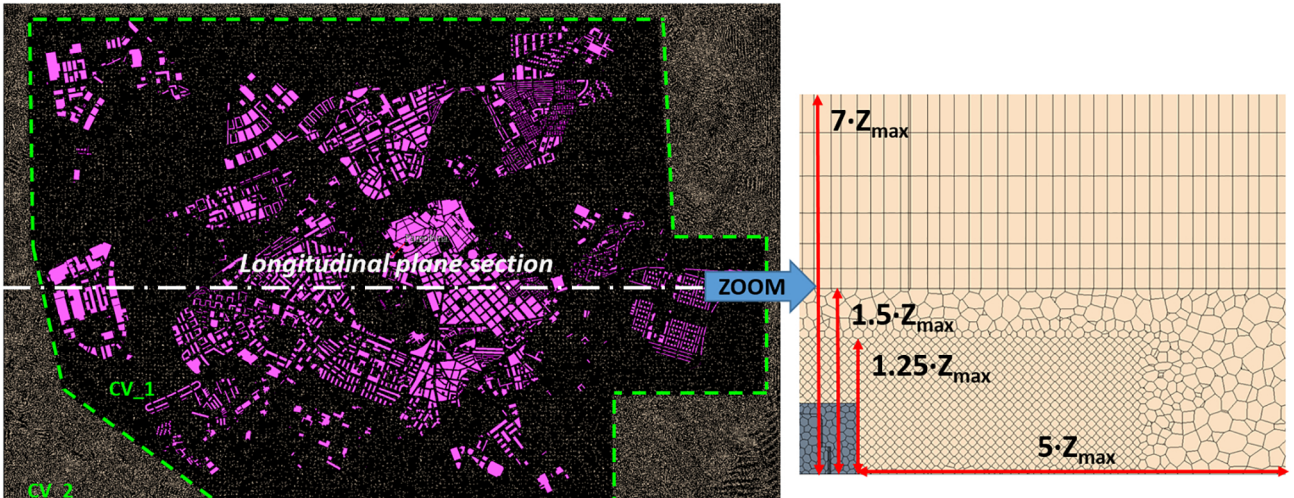
Longitudinal plane section
CV_1
CV_2
ZOOM
7·Z_max
1.5·Z_max
1.25·Z_max
5·Z_max

Figure 6

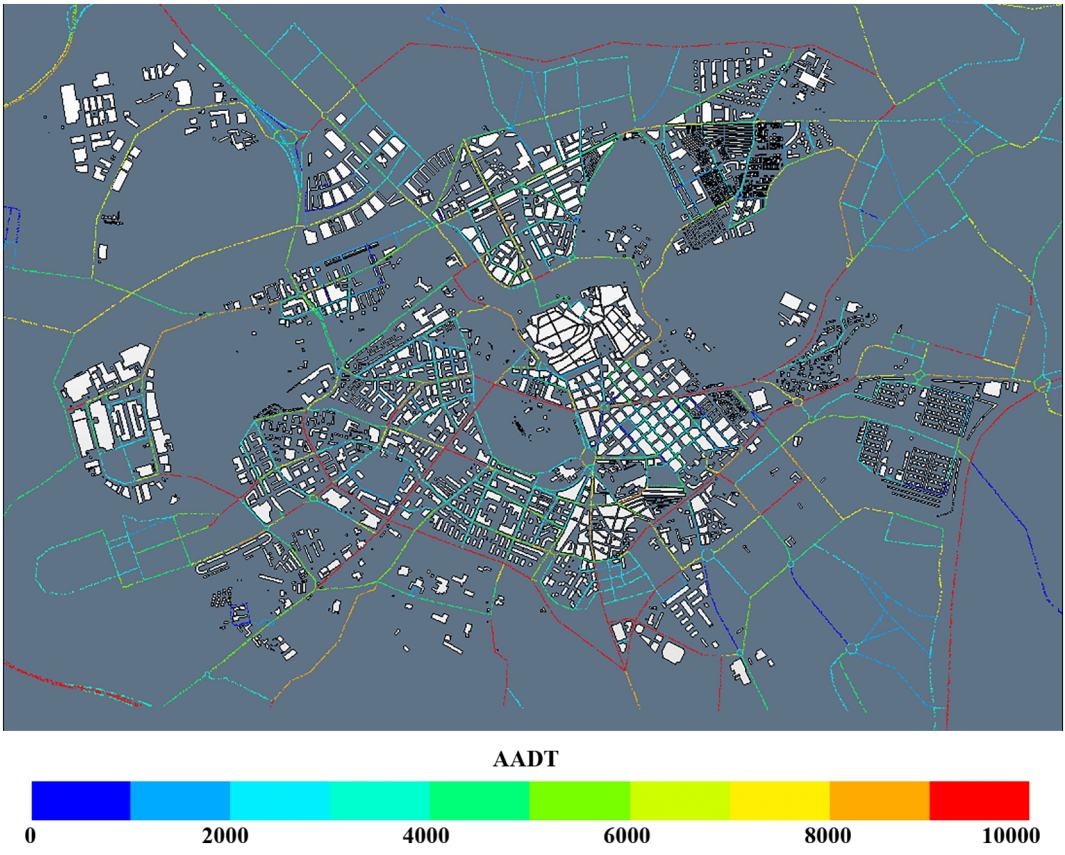

Figure 7

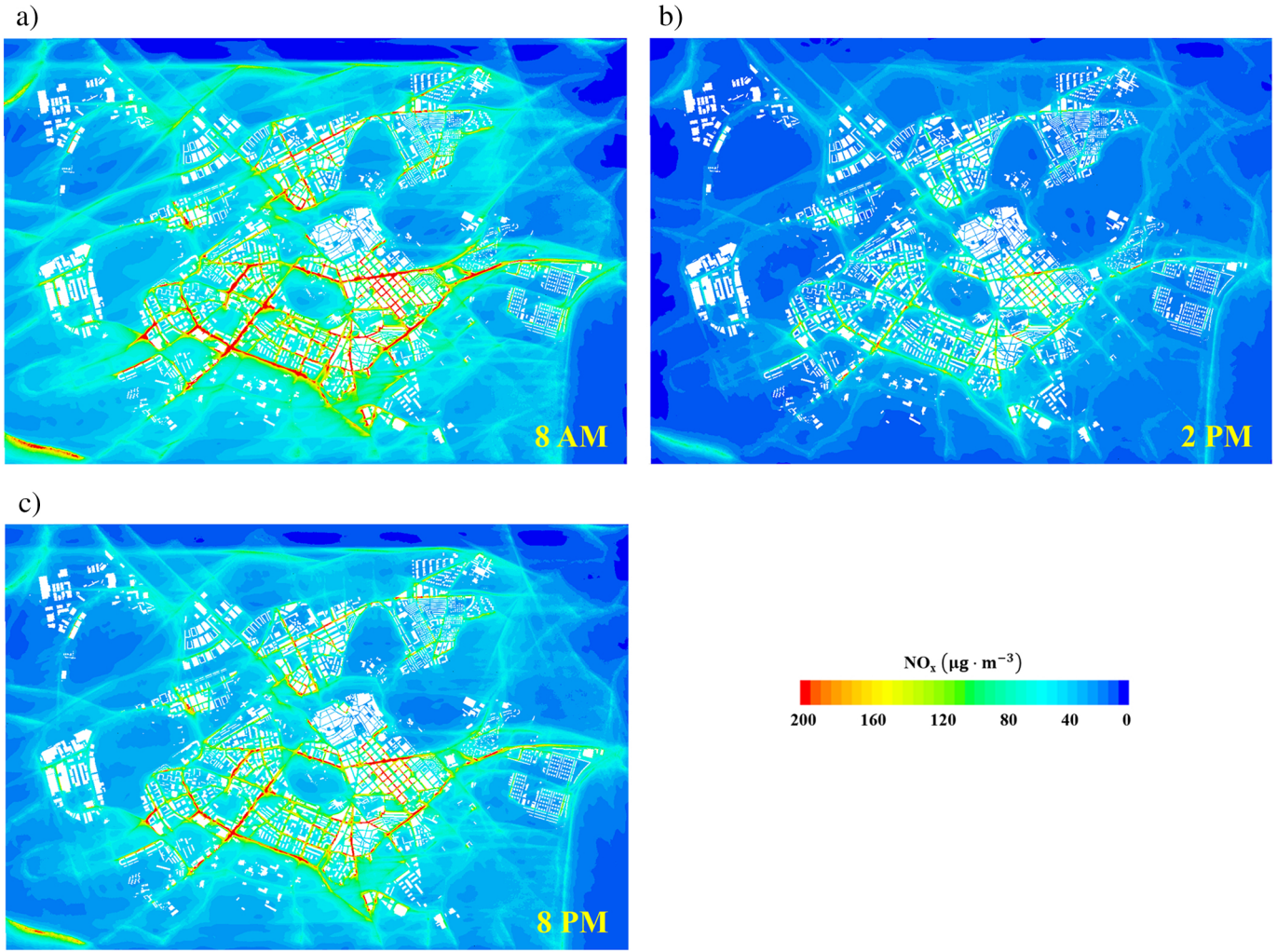

Figure 8

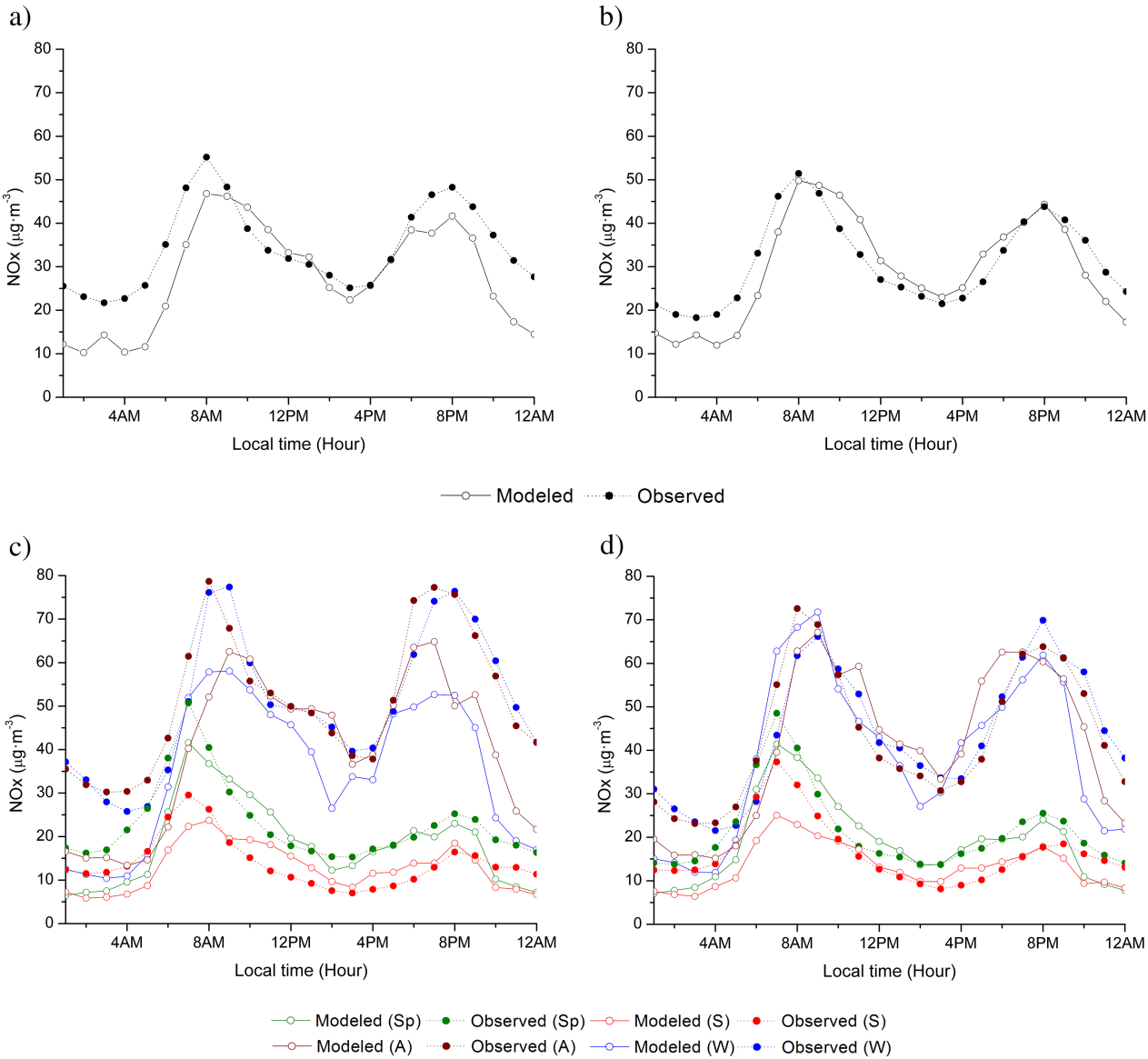
a)
b)
c)
d)
NOx (μg·m-3)
Local time (Hour)
4AM
8AM
12PM
4PM
8PM
12AM
Modeled
Observed
Modeled (Sp)
Observed (Sp)
Modeled (S)
Observed (S)
Modeled (A)
Observed (A)
Modeled (W)
Observed (W)

Figure 9

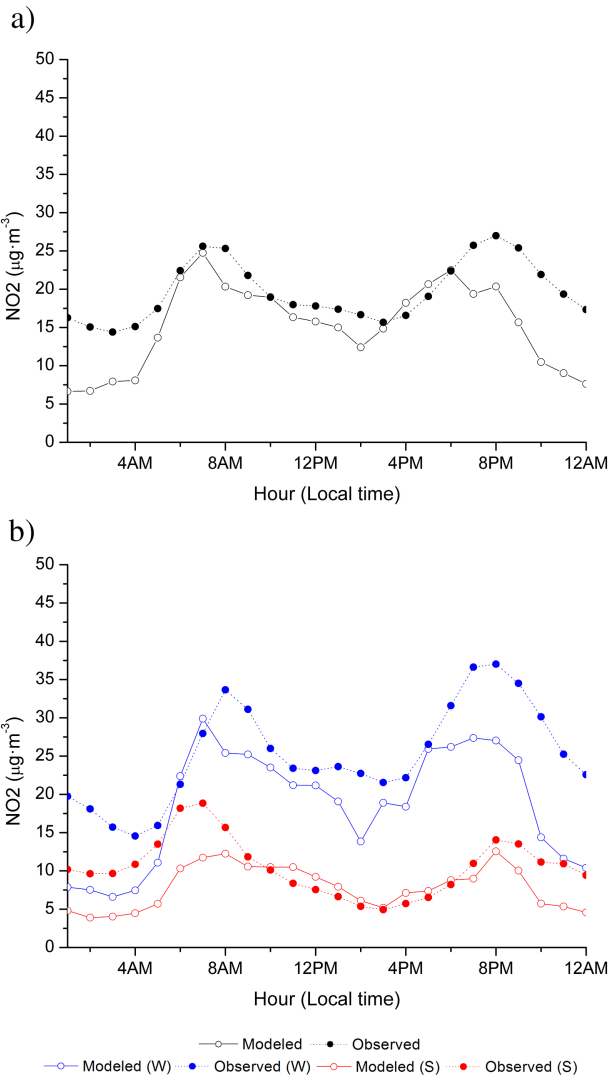
a)
NO2 (μg·m-3)
50
45
40
35
30
25
20
15
10
5
0
4AM
8AM
12PM
4PM
8PM
12AM
Hour (Local time)
b)
NO2 (μg·m-3)
50
45
40
35
30
25
20
15
10
5
0
4AM
8AM
12PM
4PM
8PM
12AM
Hour (Local time)
Modeled
Observed
Modeled (W)
Observed (W)
Modeled (S)
Observed (S)

Figure 10

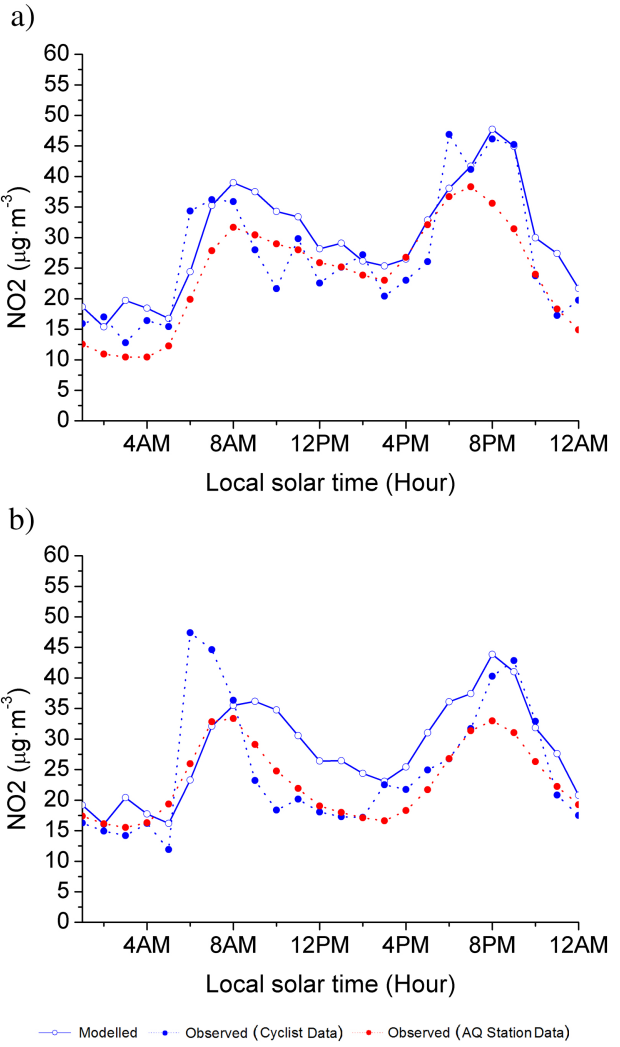
a)
NO2 (μg·m-3)
0
5
10
15
20
25
30
35
40
45
50
55
60
4AM
8AM
12PM
4PM
8PM
12AM
Local solar time (Hour)
b)
NO2 (μg·m-3)
0
5
10
15
20
25
30
35
40
45
50
55
60
4AM
8AM
12PM
4PM
8PM
12AM
Local solar time (Hour)
Modelled
Observed (Cyclist Data)
Observed (AQ Station Data)

Figure 11

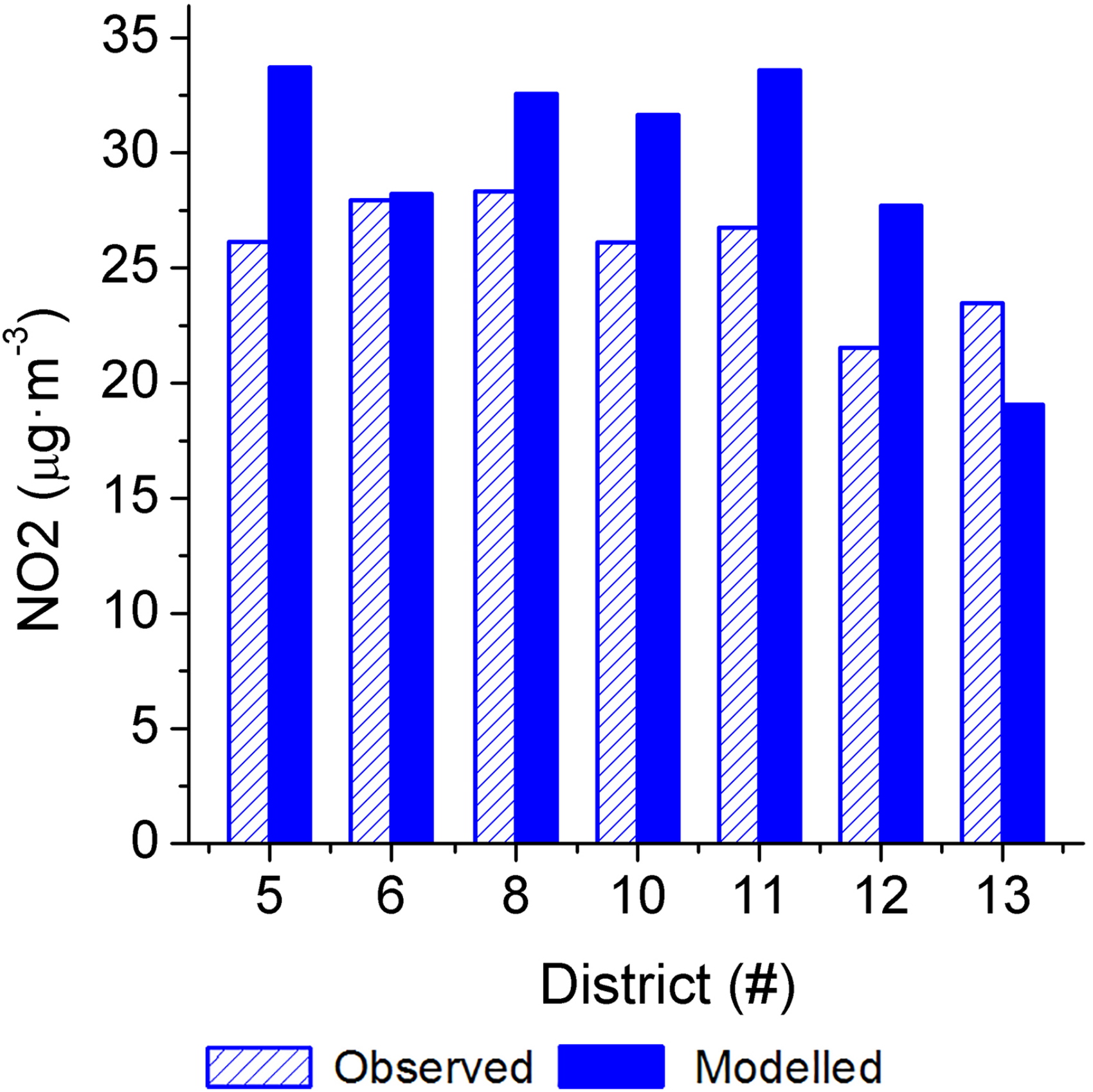
35
30
25
20
15
10
5
0
NO2 (μg·m-3)
5
6
8
10
11
12
13
District (#)
Observed
Modelled

Figure 12

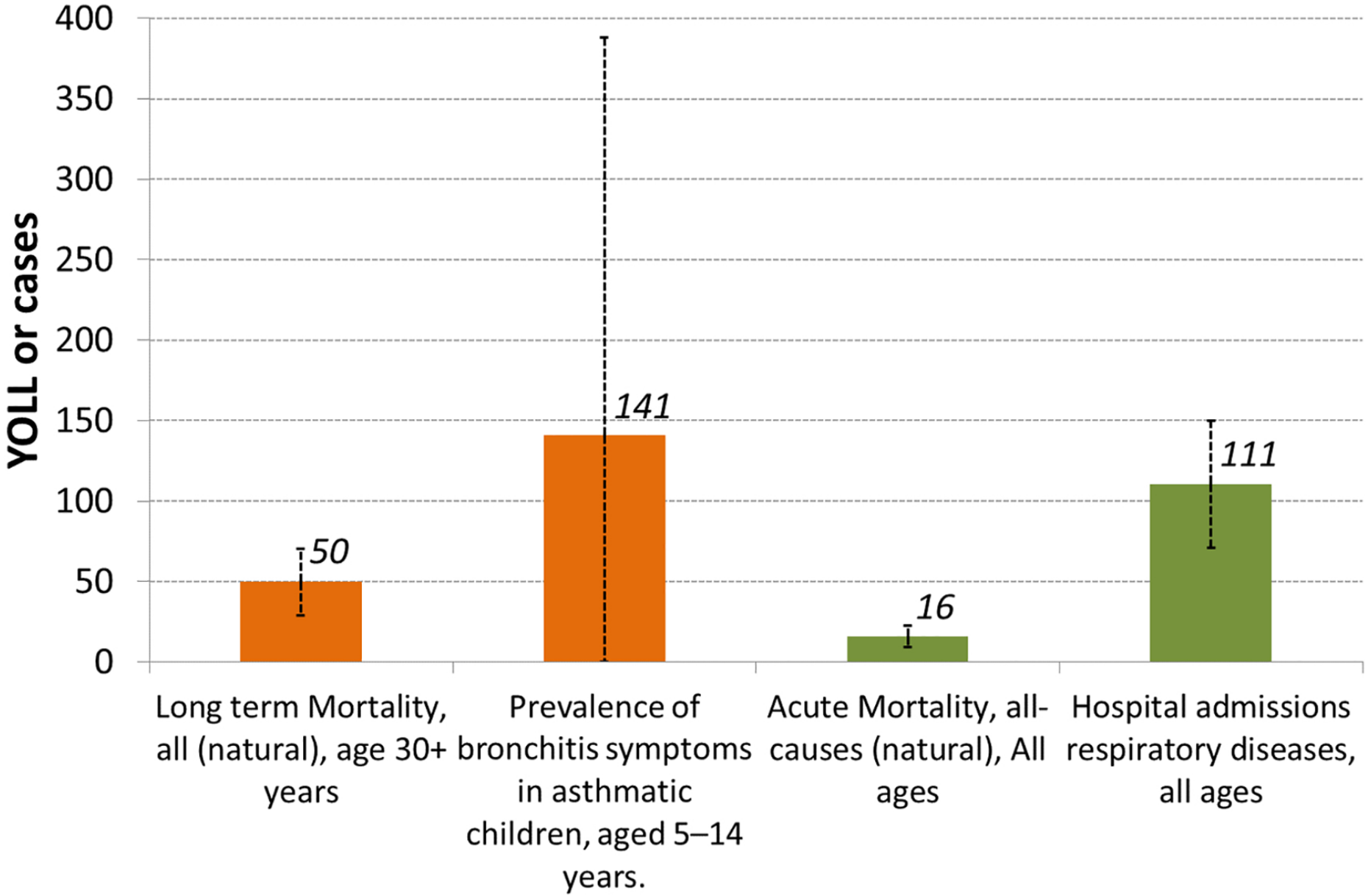
YOLL or cases
400
350
300
250
200
150
100
50
0
50
141
16
111
Long term Mortality, all (natural), age 30+ years
Prevalence of bronchitis symptoms in asthmatic children, aged 5–14 years.
Acute Mortality, all-causes (natural), All ages
Hospital admissions respiratory diseases, all ages

Figure 13

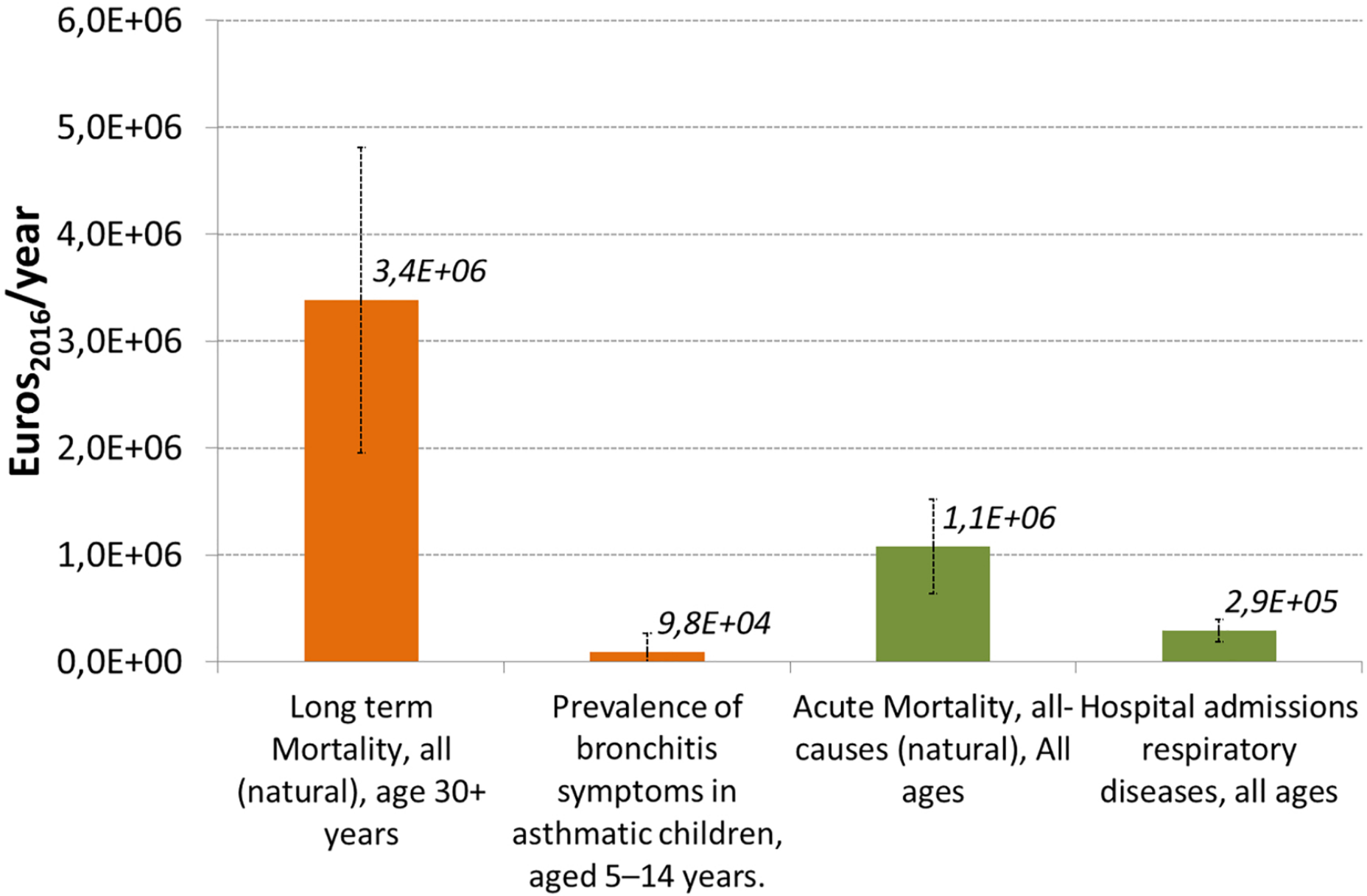
6,0E+06
5,0E+06
4,0E+06
3,0E+06
2,0E+06
1,0E+06
0,0E+00
Euros2016/year
3,4E+06
9,8E+04
1,1E+06
2,9E+05
Long term Mortality, all (natural), age 30+ years
Prevalence of bronchitis symptoms in asthmatic children, aged 5–14 years.
Acute Mortality, all-causes (natural), All ages
Hospital admissions respiratory diseases, all ages

Figure 14

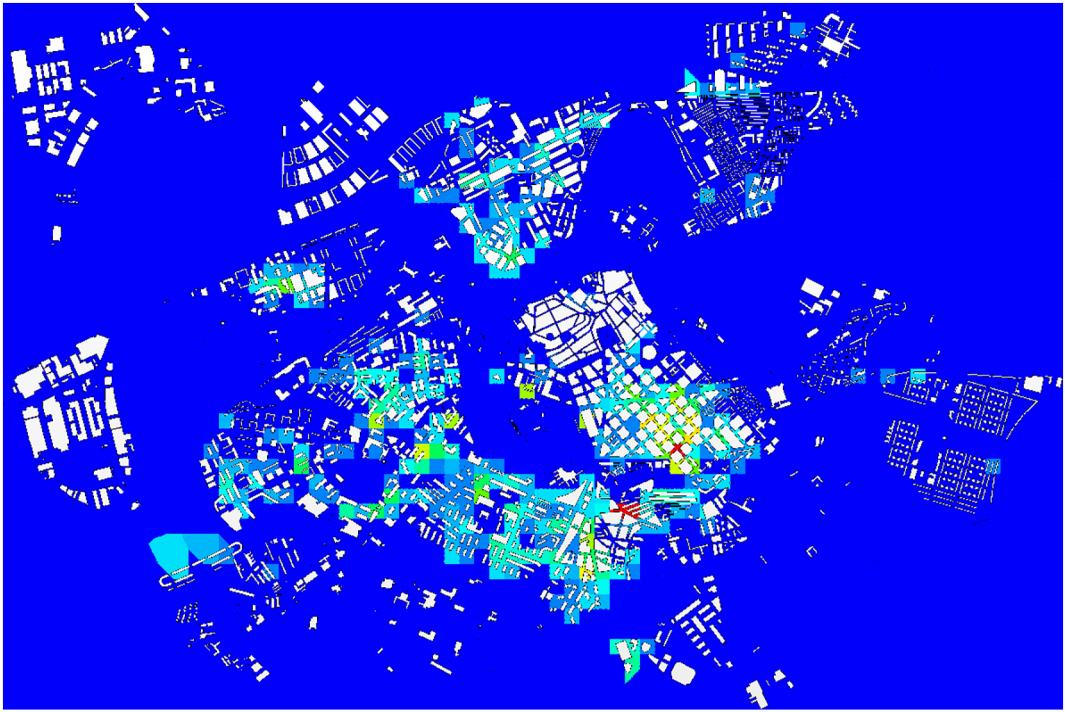

Figure 15

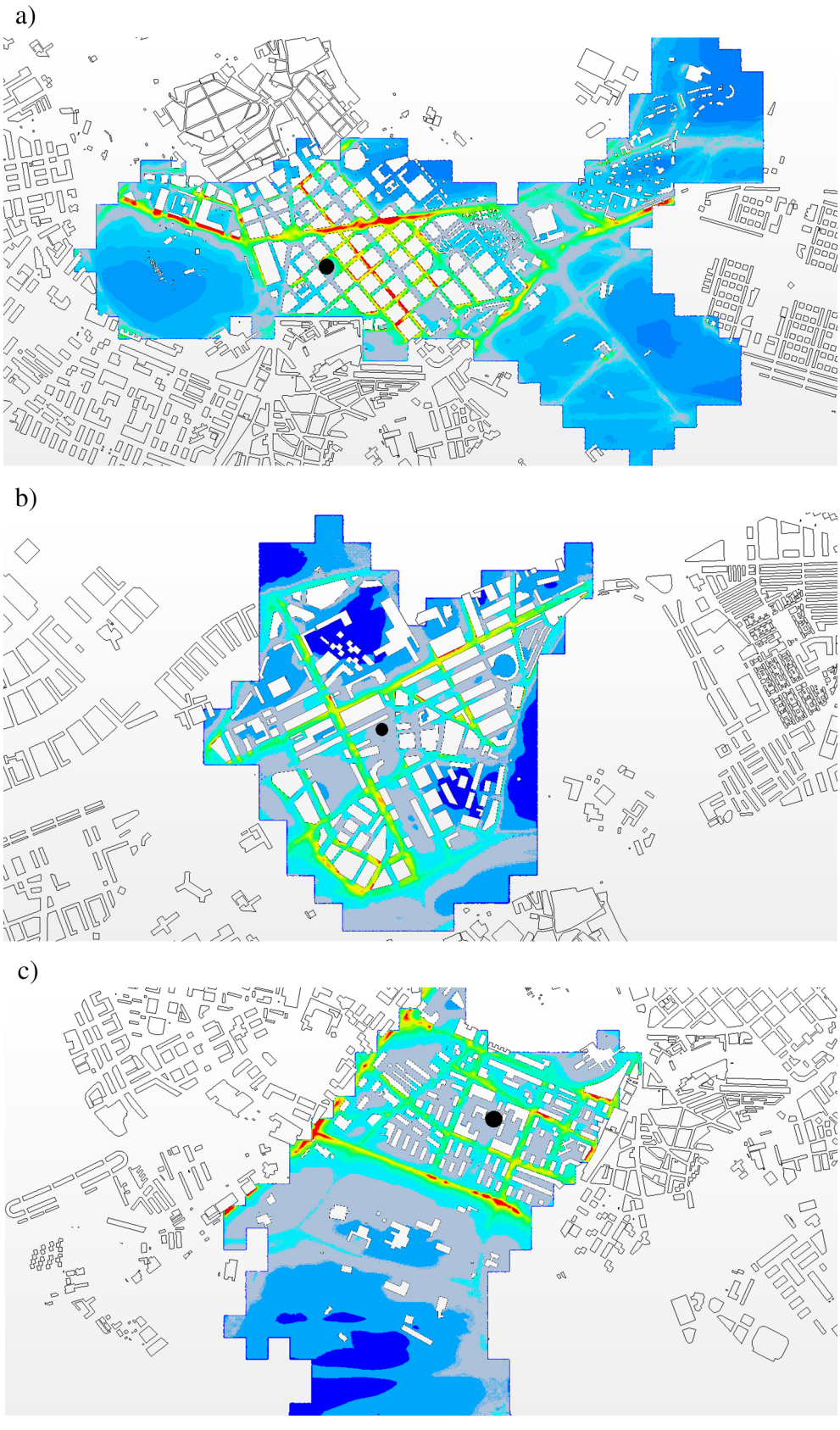

Figure 16

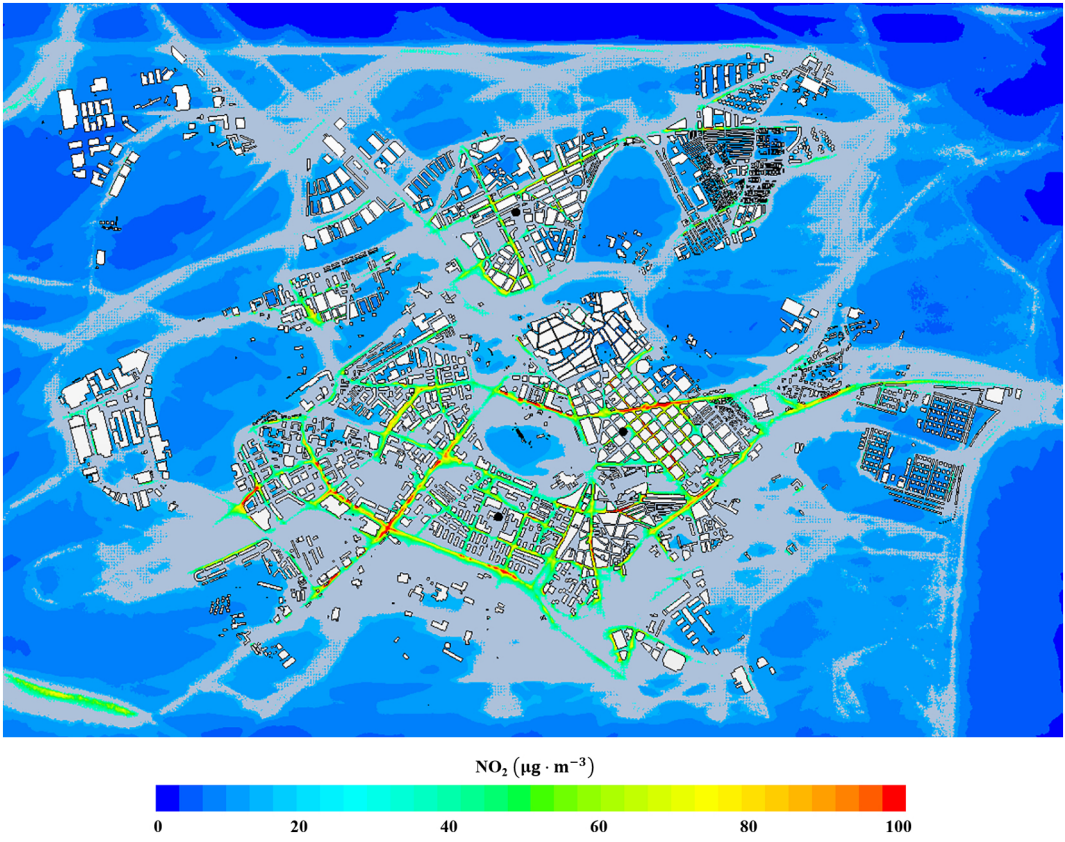

Figure 17